Hybrid Beamforming Design and Resource Allocation for UAV-aided Wireless-Powered Mobile Edge Computing Networks with NOMA

Wanmei Feng, Jie Tang, *Senior Member, IEEE*, Nan Zhao, *Senior Member, IEEE*,

Xiuyin Zhang, *Senior Member, IEEE*, Xianbin Wang, *Fellow, IEEE*,

Kai-Kit Wong, *Fellow, IEEE* and Jonathon Chambers, *Fellow, IEEE*

Abstract

Beamforming and non-orthogonal multiple access (NOMA) serve as two potential solutions for achieving spectral efficient communication in the fifth generation and beyond wireless networks. In this paper, we jointly apply a hybrid beamforming and NOMA techniques to an unmanned aerial vehicle (UAV)-carried wireless-powered mobile edge computing (MEC) system, within which the UAV is equipped with a wireless power charger and the MEC platform delivers energy and computing services to Internet of Things (IoT) devices. Our aim is to maximize the sum computation rate at all IoT devices whilst satisfying the constraint of energy harvesting and coverage. The resultant optimization problem is non-convex involving joint optimization of the UAV's 3D placement and hybrid beamforming matrices as well as computation resource allocation in both partial and binary offloading patterns, and thus is quite difficult to tackle directly. By applying the polyhedral annexation method and the deep deterministic policy gradient (DDPG) algorithm, we develop an effective algorithm to derive the closed-form solution for the optimal 3D deployment of the UAV, and find the solution for the hybrid beamformer. Two resource allocation algorithms for partial and binary offloading patterns are thereby proposed. Simulation results verify that our designed algorithms achieve a significant computation performance enhancement as compared to the benchmark schemes.

Index Terms

Hybrid beamforming, mobile edge computing, non-orthogonal multiple access, unmanned aerial vehicle, wireless power transfer

I. INTRODUCTION

The fast proliferation in the Internet-of-Things (IoT) applications has fuelled an exponential growth of IoT devices, including smartphones, wearable devices and wireless sensors, which are widely deployed to support diverse smart applications (e.g., smart cities, automatic manufacturing and smart homes) [1]. However, many of these intelligent applications, such as augmented reality and autonomous navigation, are computationally-intensive and latency-sensitive, which are extremely difficult for IoT devices to handle due to their limited computing capacity. Mobile edge computing (MEC) can potentially serve as an effective technique for enhancing the computing capacity of IoT devices through offloading. With MEC, the IoT devices can offload partial or entire computation missions to the computing servers that are located at the network edge, for instance the base stations (BSs) [2], [3]. In particular, there are two types of working modes in the MEC paradigms, partial and binary offloading. In the partial offloading pattern, the computation missions at IoT devices are partitioned into two parts, one of which is processed locally at the IoT devices whilst the other part is transmitted for edge execution. In the binary offloading pattern, the entire computation missions are accomplished either at the IoT devices or at the nearby MEC servers [2], [3].

Recently, non-orthogonal multiple access (NOMA) has been viewed as a potential technique for the fifth generation (5G) and beyond 5G (B5G) wireless networks [4], [5]. It has been confirmed that combining MEC and NOMA can reduce the latency and energy cost, and therefore enhance the performance of computation offloading in the MEC paradigms [6]–[8]. In [6], by applying the multi-antenna NOMA technique, weighted sum-energy minimization problems in two working modes were studied in multiuser MEC networks, where the user's central processing unit (CPU) frequencies and transmit power as well as the rate for offloading were jointly optimized. The authors in [7] aimed at minimizing the completion time and energy expenditure of all users in a NOMA-based uplink MEC network. In [8], a framework for computation efficiency had studied in a distributed NOMA-based MEC network, and solved by the Dinkelbach-based iterative algorithm and Karush-Kuhn-Tucker (KKT) conditions, respectively. Nevertheless, when the IoT devices are placed in an area where communication facilities are sparsely distributed, it is not efficient for MEC servers to provide computing services.

Due to the advantages of autonomy, flexibility and mobility, unmanned aerial vehicles (UAVs) can be rapidly deployed for providing reliable services for users in rural and geographically constrained areas [9]. Therefore, the application of UAVs within MEC networks can eliminate the aforementioned shortcomings since they can further shorten the transmission distance and increase the channel gain

[10]–[13]. In [10], a total energy minimization problem was studied in a UAV-aided MEC system, where computation resource allocation and UAV trajectory design were considered. A penalty dual decomposition (PDD)-based algorithm was studied in [11] to minimize the maximum task completion time in UAV-aided MEC systems. An alternating optimization scheme for a multiuser aerial MEC system was proposed in [12] to minimize the energy cost, in which the location of the UAV, the time allocation and the task partition were taken into account. Based on the aforementioned research on single UAV solutions, a two-layer optimization scheme for a multi-UAV-aided MEC system was investigated in [13] to reduce the energy expenditure, where the UAV position and task assignment were optimized.

On the other hand, the wireless power transfer (WPT) has been viewed as a potential technique to prolong the battery-life of IoT devices [14], [15]. Therefore, the integration of MEC and WPT can enhance the computing capacity of IoT devices due to the extension of MEC service time [2], [16]–[18]. In [2], a coordinate descent method and an alternating direction method were exploited to maximize the weighted sum computation rate of the system in a multi-user wireless-powered MEC network. Two alternative schemes were designed in [16] to maximize the weighted sum computation rates of users by considering the CPU frequencies, the offloaded time and the transmission power as well as the UAV's trajectory in a UAV-aided MEC wireless-powered system. This work has been recently extended in [17] to achieve the computation efficiency enhancement in a wireless-powered MEC network, in which energy harvesting time, CPU frequencies, upload time and transmission power were jointly optimized. A successive convex approximation (SCA) method and an iterative algorithm were proposed in [18] to minimize the consumed energy in a UAV-aided wireless-powered MEC system.

In fact, although the computation performance of IoT devices can be improved by WPT, the performance gain is very limited. This is because the harvested energy is significantly degraded by the severe path loss. To tackle this problem, energy beamforming is used to focus the transmitted energy on the receivers for improving the energy transfer efficiency. However, few works have focused on applying the beamforming technique within wireless-powered MEC networks [19]. By applying the maximum ratio transmission (MRC) energy beamforming technique, the authors in [19] investigated the transmission energy consumption minimization framework in a wireless-powered MEC system.

A. Main Contributions

Previous works focus on studying the resource allocation problem for NOMA-aided MEC networks [6]–[8], where the UAVs and WPT are not considered to provide energy supply and computing services for cell-edge users. On the other hand, the works in [10]–[13] aim to minimize the energy expenditure and latency in UAV-aided MEC networks, but do not exploit the NOMA and the WPT for improving the computing capacity of IoT devices. In addition, the works in [2], [16]–[18] focus on investigating the resource management schemes in UAV-aided wireless-powered MEC systems, which cannot simultaneously support multiple users offloading their tasks to computing systems. The work in [19] proposed to apply the energy beamforming within wireless power MEC networks. However, this framework cannot be directly used to more general multi-user environments since only a single user is considered. Motivated by the aforementioned observations, we consider a hybrid beamforming design and resource allocation for sum computation rate maximization in a multiuser UAV-aided wireless-powered MEC network. Our contributions are summarized as follows.

- We formulate the design of hybrid beamforming and resource allocation for IoT devices in a UAV-aided wireless-powered MEC network under partial and binary offloading patterns. We aim to maximize the sum computation rate at all IoT devices while satisfying the constraint of energy harvesting and coverage. The considered optimization problem is non-convex involving joint optimization of the UAV's 3D placement and the hybrid beamforming matrices as well as computation resource allocation, which is quite difficult to tackle directly. Thus, we first design the 3D placement of the UAV and hybrid beamforming matrices, and then two resource allocation algorithms for the corresponding computation modes are presented.

- For the 3D placement and hybrid beamforming design, we first formulate the energy harvesting maximization problem with the coverage constraint as a convex maximization problem. By applying the polyhedral annexation method, we design the sequential unconstrained convex minimization (SUCM) based placement optimization algorithm to achieve the optimal 3D placement of the UAV. After that, a learning-based two stage hybrid beamforming scheme is proposed to optimize the hybrid beamforming matrices.

- In the case of partial offloading, the sum computation rate maximization problem is expressed as a mixed combinatorial non-convex optimization problem. Inspired by the alternative optimization method and Lagrange dual method, we propose an effective resource allocation scheme to tackle this problem.

- In the case of binary offloading, we develop a resource allocation scheme to handle the decision variables in an iterative manner for a given mode selection decision. Furthermore, by applying the bisection method, we present a channel-gain-based mode selection algorithm to optimize the computing modes.

- Numerical results verify that significant computation performance gain can be achieved through our proposed algorithms as compared to the benchmark schemes, thereby demonstrating the advantages of integrating hybrid beamforming and the NOMA into UAV-aided wireless-powered MEC networks.

B. Organization and Notation

The remainder of this paper is organized as follows. The system model and the sum computation rate maximization problem under the partial and binary offloading are proposed in Section II. In Section III, a SUCM-based placement optimization algorithm and a learning-based two stage hybrid beamforming design are proposed. Two resource allocation algorithms for the partial and binary offloading are discussed in Section IV and Section V, respectively. Numerical results and the conclusion are discussed in Section VI and Section VII.

The following notations are used in this paper. $\mathbf{A}$ is a matrix. $\mathbf{a}^T$ and $\mathbf{a}^H$ denote the transpose and complex conjugate transpose of the vector $\mathbf{a}$. $\|\mathbf{a}\|$ denotes the Euclidean norm. In addition, $\mathbf{R}_+(\mathbf{R}_-)$ represents the set of nonnegative (negative) real numbers.

II. SYSTEM MODEL AND PROBLEM FORMULATION

A. System Model

As depicted in Fig. 1, we consider a UAV-aided wireless powered MEC system with a UAV and K IoT devices, where the UAV is setup with an $M \times N$ rectangular antenna array and all IoT devices have single antenna. In particular, the UAV is mounted with a radio frequency (RF) energy transmitter and a communication unit as well as an MEC server, while each device is mounted with an energy harvesting unit, a communication unit as well as a computation unit [2]. The computation unit of each device is a micro-processor that can only perform simple tasks [2], [16].

It is assumed that all devices need to complete a certain computing task during a given period T. As shown in Fig. 2, a harvest-then-offload protocol is exploited, in which the whole period T contains three phases. In the first phase with duration aT ($a \in [0, 1]$), the UAV generates multi-beams
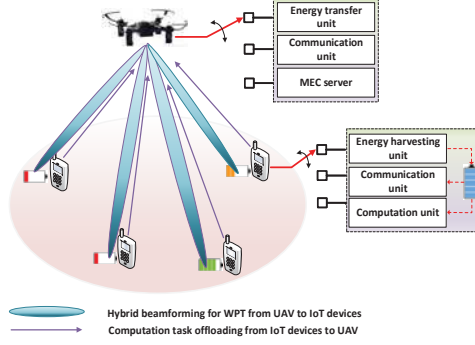
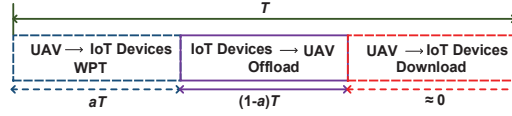**Fig. 1:** Illustration of a multiuser UAV-aided wireless powered MEC system with hybrid beamforming.

Fig. 2: A harvest-then-offload protocol in the UAV-aided wireless powered MEC system.

to broadcast wireless energy to all IoT devices. Subsequently, IoT devices store the RF energy with the energy harvesting unit, and then transmit the computation tasks to the UAV platform in the second phase with time duration $(1-a)T$. After receiving the offloaded tasks, the UAV executes and replies to the corresponding devices during the third phase. Since the computing capacity of the UAV is much greater than the IoT devices, the data processing and downloading time for the UAV is neglected [2].

In general, the UAV's 2D horizontal location is denoted as $z_u = (x_u, y_u)$, with its altitude as h_u. The location of the device k on the ground is denoted as $z_k = (x_k, y_k)$, where $k \in \mathcal{M} = \{1, 2, \cdots K\}$. The UAV can be flexibly deployed and fly at relatively high altitudes, such that the UAV-ground channels are characterized by line-of-sight (LoS) links. Thus, the channel between the UAV and device k is given by [9]

$$\mathbf{h}_k = \sqrt{\beta_0 d_k^{-\alpha}} \mathbf{a}(\theta, \phi), \tag{1}$$

where α ($\alpha \geq 2$) and $d_k = \sqrt{(x_k - x_u)^2 + (y_k - y_u)^2 + h_u^2}$ indicate the path loss exponent and the distance between the UAV and the device k, respectively. Also, β_0 is the channel power gain at the reference distance of $d_0 = 1$ m. Let the wavelength and the spacing between antenna elements be denoted by λ and d_{array}. The steering vector $\mathbf{a}(\theta, \phi)$ of an $M \times N$ antenna array can be further represented by [9]

$$\mathbf{a}(\theta, \phi) = [1, \cdots, e^{j2\pi/\lambda d_{array} \sin(\theta)[(m-1)\cos(\phi)+(n-1)\sin(\phi)]},$$
$$\cdots, e^{j2\pi/\lambda d_{array} \sin(\theta)[(M-1)\cos(\phi)+(N-1)\sin(\phi)]}]^T, \tag{2}$$
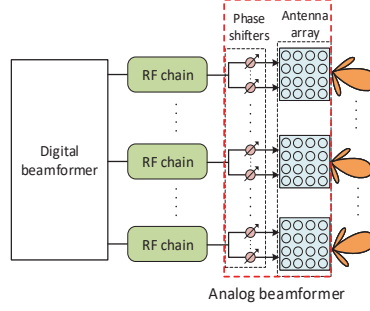
Fig. 3: A hybrid beamforming structure for energy beamforming.

where m and n represent the indices of the antenna elements in the xy-plane, respectively, and (θ, ϕ) represents the steering angles.

In practice, the number of RF chains supported at the transmitters is much less than the number of antennas due to hardware constraints [20]. Thus, we consider a hybrid beamforming structure for energy beamforming at the UAV, as shown in Fig. 3, which consists of an analog beamformer and a digital beamformer [21]. The antenna array is partitioned into several sub-arrays, wherein each RF chain is connected to a sub-array and the number of antenna elements per sub-array is N_a^t. It is assumed that the total number of RF chains in the hybrid beamforming architecture is equal to the number of IoT devices, i.e, $N_{RF} = K$. The total number of antenna elements can be calculated by $M \cdot N = N_{RF} \cdot N_a^t$. Then, the channel power gain from the UAV to the device k is expressed as

$$|\mathbf{h}_k^H \mathbf{F} \mathbf{w}_k|^2 = \frac{\beta_0}{[(x_k - x_u)^2 + (y_k - y_u)^2 + h^2]^{\alpha/2}} |\mathbf{B}_k|^2, \tag{3}$$

where $\mathbf{B}_k = \mathbf{a}^H(\theta, \phi)\mathbf{F}\mathbf{w}_k$ and $\mathbf{W} = [\mathbf{w}_1, \mathbf{w}_2, \cdots, \mathbf{w}_K]^T$ denotes the $N_{RF} \times K$ digital beamforming matrix. $\mathbf{F}$ represents the analog beamforming matrix given by

$$\begin{bmatrix} \mathbf{a}(\theta_1, \phi_1) & \mathbf{0}_{N_a^t} & \cdots & \mathbf{0}_{N_a^t} \\ \mathbf{0}_{N_a^t} & \mathbf{a}(\theta_2, \phi_2) & \cdots & \mathbf{0}_{N_a^t} \\ \vdots & \vdots & \ddots & \vdots \\ \mathbf{0}_{N_a^t} & \mathbf{0}_{N_a^t} & \cdots & \mathbf{a}(\theta_{N_{RF}}, \phi_{N_{RF}}) \end{bmatrix}. \tag{4}$$

The diagonal entry $\mathbf{f}_i = \mathbf{a}(\theta_i, \phi_i)$ refers to the analog steering vector for the ith sub-array, $i \in \{1, 2, \cdots, N_{RF}\}$, and (θ_i, ϕ_i) corresponds to the designed steering angles.

Note that the harvested energy at device k can be shown to be

$$E_k = \tau_0 \xi_0 P_0 |\mathbf{h}_k^H \mathbf{F} \mathbf{w}_k|^2, \tag{5}$$

where P_0 indicates the transmit power of the UAV and τ_0 represents the energy harvesting time. $\xi_0 (0 < \xi_0 < 1)$ denotes the energy conversion efficiency.

B. Partial Offloading

1) Local Computing: Similar to [2], [16], IoT devices can perform local computation and task offloading as well as harvesting energy simultaneously since the energy harvesting unit, communication unit and the computation unit are separated. Let the number of computation cycles required for executing one bit of raw data be denoted by C. We denote the CPU frequency of device k as f_k, which holds $f_k \le f_{max}$. The computation rate of device k is expressed as

$$r_{L,k}^{Par} = \frac{f_k t_k}{CT}, \ \ k \in \mathcal{M}, \tag{6}$$

where $0 < t_k < T$ is the computation time of the kth device. Accordingly, the consumed energy at device k is given by

$$E_{L,k}^{Par} = \tau_k f_k^3 t_k, \ \ k \in \mathcal{M}, \tag{7}$$

where τ_k denotes the effective capacitance coefficient.

2) Offloading Computation: Instead of time division multiple access (TDMA), we apply the NOMA scheme that enables all the IoT devices to send tasks to the UAV simultaneously [22], [23]. The channel power gain from the kth device to the UAV is written as [18]

$$g_k = \frac{\beta_0}{[(x_k - x_u)^2 + (y_k - y_u)^2 + h_u^2]^{\alpha/2}}. \tag{8}$$

Without loss of generality, the channel power gains between IoT devices and the UAV are arranged in an ascending order $g_1 < g_2 < \cdots < g_K$. Let B and P_k denote the communication bandwidth and the transmit power of the kth device. The achievable offloading rate from the kth device to the UAV under a given period $(1-a)T$ is then given by

$$r_{o,k}^{Par} = \begin{cases} B(1-a)\log_2\left(1 + \dfrac{P_k g_k}{\sum_{i=k+1}^{K} P_i g_i + N_0}\right), 1 \le k \le K-1, \\ B(1-a)\log_2\left(1 + \dfrac{P_k g_k}{N_0}\right), k = K, \end{cases} \tag{9}$$

where N_0 represents the receiver noise power. Thus, from (6) and (9), the total computation rate of device k is expressed as

$$r_{o,k}^{Par} = \begin{cases} \dfrac{f_k t_k}{CT} + B(1-a)\log_2\left(1 + \dfrac{P_k g_k}{\sum_{i=k+1}^{K} P_i g_i + N_0}\right), 1 \le k \le K-1, \\[2ex] \dfrac{f_k t_k}{CT} + B(1-a)\log_2\left(1 + \dfrac{P_k g_k}{N_0}\right), k = K. \end{cases} \quad (10)$$

Since the energy consumed by the IoT devices during task execution comes from the harvested energy, it needs to satisfy the following energy harvesting constraints

$$\tau_k f_k^3 t_k + P_k(1-a)T \le aT\xi_0 P_0 |\mathbf{h}_k^H \mathbf{F} \mathbf{w}_k|^2, k \in \mathcal{M}, \quad (11)$$

$$aT\xi_0 P_0 |\mathbf{h}_k^H \mathbf{F} \mathbf{w}_k|^2 \le T\xi_0 P_0 |\mathbf{h}_k^H \mathbf{F} \mathbf{w}_k|^2 \le \tau_k f_{max}^3 T, k \in \mathcal{M}. \quad (12)$$

From (12), it can be shown that the harvested energy can be drained when the IoT devices operate at the maximum computing speed [2].

C. Binary Offloading

Let the set of IoT devices operate in local computation and task offloading be denoted by $\mathcal{M}_0 = \{1, \cdots, l_0\}$ and $\mathcal{M}_1 = \{1, \cdots, l_1\}$, where $\mathcal{M} = \mathcal{M}_0 \cup \mathcal{M}_1 = \{1, \cdots, K\}$ and $\mathcal{M} = \mathcal{M}_0 \cap \mathcal{M}_1 = \{\emptyset\}$.

1) Local Computing: For device $k \in \mathcal{M}_0$, all the accumulated energy is exploited for local computation. The computation rate and consumed energy of device k can be expressed as

$$r_{L,k}^{bin} = \frac{f_k t_k}{CT}, \quad \forall k \in \mathcal{M}_0, \quad (13)$$

$$E_{L,k}^{bin} = \tau_k f_k^3 t_k, \quad \forall k \in \mathcal{M}_0. \quad (14)$$

2) Offloading Computation: In this case, each device in $\mathcal{M}_1$ consumes all the accumulated energy to transmit their tasks to the UAV for edge computing. The achievable offloading rate from the kth device to the UAV is written as

$$r_{o,k}^{bin} = \begin{cases} B(1-a)\log_2\left(1 + \dfrac{P_k g_k}{\sum_{i=k+1}^{K} P_i g_i + N_0}\right), 1 \le k \le K-1, \\[2ex] B(1-a)\log_2\left(1 + \dfrac{P_k g_k}{N_0}\right), k = K. \end{cases} \quad (15)$$

Correspondingly, the energy harvesting constraints are given by

$$\tau_k f_k^3 t_k \le aT\xi_0 P_0 |\mathbf{h}_k^H \mathbf{F} \mathbf{w}_k|^2, k \in \mathcal{M}_0, \quad (16)$$

$$P_k(1-a)T \leq aT\xi_0 P_0 |\mathbf{h}_k^H \mathbf{F}\mathbf{w}_k|^2, k \in \mathcal{M}_1. \tag{17}$$

D. Problem Formulation

1) Partial Offloading: First, we consider the case of the partial offloading mode, and the sum computation rate maximization problem can be written as

$$(\text{P1}): \max_{\substack{x_u, y_u, h_u, \mathbf{W}, \mathbf{F}, \\ a, P_k, t_k, f_k}} \sum_{k \in \mathcal{M}} \left[\frac{f_k t_k}{CT} + B(1-a)\log_2\left(1 + \frac{P_k g_k}{\sum_{i=k+1}^{K} P_i g_i + N_0}\right) \right] \tag{18a}$$

$$\text{s.t.} \ \tau_k f_k^3 t_k + P_k(1-a)T \leq aT\xi_0 P_0 |\mathbf{h}_k^H \mathbf{F}\mathbf{w}_k|^2, k \in \mathcal{M}, \tag{18b}$$

$$\|z_k - z_u\|^2 \leq h_u^2 \tan^2 \Theta, \tag{18c}$$

$$h_{min} \leq h_u \leq h_{max}, \tag{18d}$$

$$0 \leq t_k \leq T, \tag{18e}$$

$$0 \leq a \leq 1, \tag{18f}$$

$$P_k \geq 0, \tag{18g}$$

$$0 \leq f_k \leq f_{max}. \tag{18h}$$

Constraint (18b) is the energy harvesting constraint for all the IoT devices. Constraint (18c) is the area coverage constraint that the horizontal distance between the IoT devices and the UAV cannot exceed $h_u \tan \Theta$, where 2Θ represents the effective illumination angle [9]. Constraint (18d) denotes the boundary constraint for the UAV's flight altitude. Constraint (18e) ensures that the computation time for IoT devices is no longer than the whole period T. Constraint (18f) is the time constraint for WPT. Constraints (18g) and (18h) correspond to the computation offloading power constraint and the CPU frequency constraint, respectively. Problem (P1) is a mixed combinatorial non-convex optimization problem due to the coupling variables.

2) Binary Offloading: Next, we consider the case in the binary offloading pattern, and the sum computation rate maximization problem can be written as

$$(\text{P2}): \max_{\substack{x_u, y_u, h_u, \mathbf{W}, \mathbf{F}, \\ a, P_k, t_k, f_k, \alpha_k}} \sum_{k \in \mathcal{M}} \left[(1-\alpha_k)\frac{f_k t_k}{CT} + \alpha_k B(1-a)\log_2\left(1 + \frac{P_k g_k}{\sum_{i=k+1}^{K} P_i g_i + N_0}\right) \right] \tag{19a}$$

$$\text{s.t.} \ \tau_k f_k^3 t_k \leq aT\xi_0 P_0 |\mathbf{h}_k^H \mathbf{F}\mathbf{w}_k|^2, k \in \mathcal{M}_0, \tag{19b}$$

$$P_k(1-a)T \leq aT\xi_0 P_0 |\mathbf{h}_k^H \mathbf{F}\mathbf{w}_k|^2, k \in \mathcal{M}_1, \tag{19c}$$

$$\|z_k - z_u\|^2 \leq h_u^2 \tan^2 \Theta, \tag{19d}$$

$$h_{min} \leq h_u \leq h_{max}, \tag{19e}$$

$$0 \leq t_k \leq T, \tag{19f}$$

$$0 \leq a \leq 1, \tag{19g}$$

$$P_k \geq 0, \tag{19h}$$

$$0 \leq f_k \leq f_{max}, \tag{19i}$$

$$\alpha_k \in \{0, 1\}. \tag{19j}$$

Constraint (19j) indicates the offloading decision of each task. $\alpha_k = 1$ denotes that the task of device k can be executed on the UAV-enabled MEC server while $\alpha_k = 0$ represents the case that the task can be executed locally. Problem (P2) is a mixed integer non-convex optimization problem, which is NP-hard in general [24].

It should be noted that the optimal solutions of (18) and (19) cannot be achieved by simultaneously optimizing all these decision variables. Thus, we focus on optimizing the variables in an alternative manner. It is observed that $|\mathbf{h}_k^H \mathbf{F} \mathbf{w}_k|^2$ can be independently adjusted to maximize the harvested energy at the IoT devices. Motivated by this, we decouple the considered problem into two subproblems, where the solutions are obtained through two steps. In the first step, the 3D placement of the UAV and the hybrid beamforming matrices should be optimized first for maximizing the harvested energy at the IoT devices. Then, based on the harvesting energy constraint, two resource allocation algorithms are properly designed to maximize the sum computation rate at the IoT devices.

III. 3D PLACEMENT FOR UAV AND HYBRID BEAMFORMING FOR WPT

Since the hybrid beamforming design needs to acquire the beam scanning angles, the UAV's 3D placement should be determined first. Therefore, we first present an effective algorithm to optimize the 3D position of the UAV. Then, we propose a learning-based two-stage hybrid beamforming design to optimize the hybrid beamforming matrices.

A. Optimal UAV 3D Placement

To determine the 3D location of the UAV, we study the following energy harvesting maximization problem:

$$(\text{P3}) : \max_{\substack{x_u, y_u, h_u, \\ \mathbf{W}, \mathbf{F}}} \quad \sum_{k=1}^{K} aT\xi_0 P_0 |\mathbf{h}_k^H \mathbf{F} \mathbf{w}_k|^2 \tag{20a}$$

$$\text{s.t. } \|z_k - z_u\|^2 \leq h_u^2 \tan^2 \Theta, \tag{20b}$$

$$h_{min} \leq h_u \leq h_{max}, \tag{20c}$$

$$\sum_{k=1}^{K} \| \mathbf{F}\mathbf{w}_k \|^2 \leq P_{th}, \tag{20d}$$

where P_{th} denotes the total transmit power budget. For given $\mathbf{W}$ and $\mathbf{F}$, problem (P3) is non-convex due to the non-convexity of 20(a), Constraints (20b) and (20d). Thus, we first focus on solving for (x_u, y_u) with fixed h_u. With $A_k = aT\xi_0 P_0 \beta_0 |\mathbf{B}_k|^2$, $\zeta_k(x_u, y_u) = (x_k - x_u)^2 + (y_k - y_u)^2 + h_u^2$ and $\eta_k(\zeta_k(x_u, y_u)) = A_k[\zeta_k(x_u, y_u)]^{-\alpha/2}$, problem (P3) is expressed as

$$(\text{P3.1}) : \max_{x_u, y_u} \quad \sum_{k}^{K} \eta_k(\zeta_k(x_u, y_u)). \tag{21}$$

Note that in problem (P3.1), $\zeta_k(x_u, y_u)$ is convex over (x_u, y_u) and $\eta(\cdot)$ is a strictly convex function and strictly decreasing on $\mathbf{R}^+$. Since $\lim_{x_u, y_u \to \infty} \zeta_k(x_u, y_u) = +\infty$ and $\lim_{\zeta_k(x_u, y_u) \to \infty} \eta_k(\zeta_k(x_u, y_u)) = 0$, it can be confirmed that problem (P3.1) is neither a convex nor concave optimization problem [25], [26]. Thus, problem (P3.1) cannot be tackled using convex optimization methods. Therefore, we propose a SUCM-based placement optimization algorithm to deal with problem (P3.1).

To facilitate the application of the SUCM-based placement optimization algorithm, we transform problem (P3.1) into problem (P3.2) by using an auxiliary variable $\mathbf{z} = [z_1, z_2, \cdots, z_K]^T$

$$(\text{P3.2}) : \max_{x_u, y_u, \mathbf{z}} \quad \sum_{k=1}^{K} \eta_k(z_k) \tag{22a}$$

$$\text{s.t. } \zeta_k(x_u, y_u) \leq z_k, \ k = 1, 2, \cdots, K. \tag{22b}$$

Denote

$$\mathcal{D} = \{\mathbf{z} \in \mathbf{R}_+^k : \zeta_k(x_u, y_u) \leq z_k, \ k = 1, 2, \cdots, K, \ \exists(x_u, y_u) \in \mathbf{R}^2\}. \tag{23}$$

From (23), problem (P3.2) can be equivalently represented as

$$(\text{P3.3}) : \max_{\mathbf{z} \in \mathcal{D}} \ \eta(\mathbf{Z}), \tag{24}$$

where $\eta(\mathbf{z}) = \sum_{k=1}^{K} \eta_k(z_k)$. Since $\eta(\mathbf{z})$ is a convex function and $\mathcal{D}$ denotes a compact convex set,

problem (P3.3) is recognized as a convex maximization problem [27].

Denote $\mathcal{C} = \{\mathbf{z} \in \mathbf{R}_+^k : \eta(\mathbf{z}) \le \eta(\mathbf{z}^*)\}$, $\widetilde{\mathcal{C}} = \{\mathbf{z} - \mathbf{z}_0 \mid \mathbf{z} \in \mathcal{C}\}$ and $\widetilde{\mathcal{D}} = \{\mathbf{z} - \mathbf{z}_0 \mid \mathbf{z} \in \mathcal{D}\}$. Here, $\mathbf{z}_0 = [z_{0,1}, z_{0,2}, \cdots, z_{0,K}]^T$ denotes a feasible point, and $\mathbf{z}^*$ is the best feasible solution. It is observed that the solutions in $\mathcal{C}$ and $\widetilde{\mathcal{C}}$ are not better than $\mathbf{z}^*$. If $\widetilde{\mathcal{D}} \subset \widetilde{\mathcal{C}}$, it follows that $\mathbf{z}^*$ is a global optimal solution; otherwise, it follows that $\mathbf{z}^*$ is a local solution. By introducing the concept of polar set[1], we have the following proposition to determine whether $\widetilde{\mathcal{D}} \subset \widetilde{\mathcal{C}}$.

Proposition 1: Let $\mathcal{V}$ denote the vertex set of the polytope $\mathcal{B}$. $\widetilde{\mathcal{C}}^\mathrm{o} \subset \widetilde{\mathcal{D}}^\mathrm{o}$ satisfies

$$\max_{\mathbf{z} \in \widetilde{\mathcal{D}}} \boldsymbol{v}^T \mathbf{z} \le 1, \ \ \forall \boldsymbol{v} \in \mathcal{V}, \tag{25}$$

where $\boldsymbol{v} = [v_1, v_2, \cdots, v_K]^T$. $\widetilde{\mathcal{C}}^\mathrm{o}$ and $\widetilde{\mathcal{D}}^\mathrm{o}$ represent the polar set of $\widetilde{\mathcal{C}}$ and $\widetilde{\mathcal{D}}$, respectively. The polytope $\mathcal{B}$ satisfies $\widetilde{\mathcal{C}}^\mathrm{o} \subset \mathcal{B} \subset \mathbf{R}_-^K$ [26].

Proof: It is noted that by applying the property of the polar set, (25) holds which implies that $\boldsymbol{v} \in \widetilde{\mathcal{D}}^\mathrm{o}$, $\forall \boldsymbol{v} \in \mathcal{V}$. Because $\mathcal{V} \subset \widetilde{\mathcal{D}}^\mathrm{o}$, $\mathcal{V} \subset \mathcal{B}$ and $\mathcal{B} \subset \widetilde{\mathcal{C}}^\mathrm{o}$, it follows that $\mathcal{B} \subset \widetilde{\mathcal{D}}^\mathrm{o}$ and $\widetilde{\mathcal{C}}^\mathrm{o} \subset \widetilde{\mathcal{D}}^\mathrm{o}$. Therefore, this completes the proof of the Proposition 1. ∎

Proposition 1 states that $\widetilde{\mathcal{D}} \subset \widetilde{\mathcal{C}}$ should satisfy (25). We use Proposition 1 and let $-\boldsymbol{v} = \boldsymbol{w} = [w_1, w_2, \cdots, w_K]^T$. Next, consider problem (P3.2) in (22) and notice that $\widetilde{\mathcal{D}} = \{\mathbf{z} - \mathbf{z}_0 \mid \mathbf{z} \in \mathcal{D}\}$, then the optimal 2D location of the UAV (x_u^*, y_u^*) can be achieved by dealing with the equivalent problem derived from (25) as

$$\min_{x_u, y_u} \ \sum_{k=1}^{K} w_k [\zeta_k(x_u, y_u) - z_{0,k}]. \tag{26}$$

By discarding the constant term $-\boldsymbol{w}^T \mathbf{z}_0$, (26) is expressed as

$$\min_{x_u, y_u} \ \sum_{k=1}^{K} w_k \left[(x_k - x_u)^2 + (y_k - y_u)^2 + h_u^2 \right]. \tag{27}$$

Thus, the closed-form expression of (x_u^*, y_u^*) from the above problem is given by

$$x_u^* = \frac{\sum_{k=1}^{K} w_k x_k}{\sum_{k=1}^{K} w_k}, \quad y_u^* = \frac{\sum_{k=1}^{K} w_k y_k}{\sum_{k=1}^{K} w_k}. \tag{28}$$

According to [26], the optimal solution of problem (P3.3) can be obtained by the polyhedral annexation procedure. In particular, we first initiate a polytope $\mathcal{B}^{(1)}$ with the vertex set $\mathcal{V}^{(1)} = \{\boldsymbol{v}^{(1)}\}$ that is

---

[1]Let the polar set Υ^o for Υ be defined as $\Upsilon^\mathrm{o} = \{\varpi \in \Psi \mid \max_{\varpi} \varpi^T x \le 1, x \in \Upsilon, \Psi \subset \mathbf{R}^n\}$ [28]. For some given subsets $\{P, G\}$, if $G^\mathrm{o} \subset P^\mathrm{o}$, it follows that $P \subset G$. Here, G^o and P^o represent the polar set of G and P.

TABLE I: THE SUCM-BASED PLACEMENT OPTIMIZATION ALGORITHM

1: Initialize polytope $\mathcal{B}^{(1)}$ with vertex set $\mathcal{V}^{(1)} = \{\boldsymbol{v}^{(1)}\}$;
   The best-feasible $\mathbf{z}^*$ satisfies $\eta(\mathbf{z}_0) \leq \eta(\mathbf{z}^*)$; Iterate index: m=1;

2: **ITERATE**
   FOR ALL $-\boldsymbol{w} \in \mathcal{V}^{(m)}$
      Calculate $-\psi(\boldsymbol{w})$ and (x_u^*, y_u^*) by solving (27)
   END

3: **IF** $\max_{-\boldsymbol{w} \in \mathcal{V}^{(m)}} -\psi(\boldsymbol{w}) + \boldsymbol{w}^T \mathbf{z}_0 \leq 1$
   RETURN;
   END

4: Calculate $\overline{\boldsymbol{w}}$ and $\overline{\mathbf{z}}$ using
   $\overline{\boldsymbol{w}} \in \max_{-\boldsymbol{w} \in \mathcal{V}^{(m)}} -\psi(\boldsymbol{w}) + \boldsymbol{w}^T \mathbf{z}_0$ and $\overline{z}_k = \zeta_k(\overline{x}_u, \overline{y}_u)$;

5: **IF** $\eta(\overline{\mathbf{z}}) > \eta(\mathbf{z}^*)$
   Update $\mathbf{z}^* = \overline{\mathbf{z}}$;
   ELSE
   Calculate ε and $\mathcal{B}^{(m+1)}$;
   END
   $m := m + 1$;

6: **UNTIL: CONVERGENCE**.

---

constructed by $\mathcal{B}^{(1)} = \left\{ \mathbf{z} \in \mathbf{R}_-^K : -\sum_{k=1}^K z_k \leq \frac{1}{\varsigma} \right\}$. The best feasible solution $\mathbf{z}^*$ satisfies $\eta(\mathbf{z}_0) \leq \eta(\mathbf{z}^*)$. Here, ς is small enough such that $\varsigma > 0$ holds, and m is the iteration index. Based on the vertex set $\mathcal{V}^{(m)}$, we calculate $-\psi(\boldsymbol{w})$ and (x_u^*, y_u^*) by solving the problem in (27), where $\psi(\boldsymbol{w})$ is the objection function value of (27). Here, if the optimal value of $\boldsymbol{w}$ satisfies $\max_{-\boldsymbol{w} \in \mathcal{V}^{(m)}} -\psi(\boldsymbol{w}) + \boldsymbol{w}^T \mathbf{z}_0 \leq 1$, it follows that $\mathbf{z}^*$ is a globally optimal solution; otherwise, it follows that $\mathbf{z}^*$ is not a globally optimal solution. Then, we separate the local solutions by the analytic center cutting plane method (ACCPM) [29]. Specifically, we compute $\overline{\boldsymbol{w}}$ and $\overline{\mathbf{z}}$ by $\overline{\boldsymbol{w}} \in \max_{-\boldsymbol{w} \in \mathcal{V}^{(m)}} -\psi(\boldsymbol{w}) + \boldsymbol{w}^T \mathbf{z}_0$ and $\overline{z}_k = \zeta_k(\overline{x}_u, \overline{y}_u)$, respectively. Here, $\overline{x}_u = \frac{\sum_{k=1}^K \overline{w}_k x_k}{\sum_{k=1}^K \overline{w}_k}$ and $\overline{y}_u = \frac{\sum_{k=1}^K \overline{w}_k y_k}{\sum_{k=1}^K \overline{w}_k}$. If $\eta(\overline{\mathbf{z}}) > \eta(\mathbf{z}^*)$, we update $\mathbf{z}^*$ by $\overline{\mathbf{z}}$. On the other hand, if $\eta(\overline{\mathbf{z}}) \leq \eta(\mathbf{z}^*)$, we determine the cutting planes ε and update the polytope $\mathcal{B}^{(m+1)}$ by computing $\varepsilon = \sup\{\rho : \eta(\mathbf{z}_0 + \rho(\overline{\mathbf{z}} - \mathbf{z}_0)) \leq \eta(\mathbf{z}^*)\}$ and $\mathcal{B}^{(m+1)} = \mathcal{B}^{(m)} \cap \left\{ \mathbf{z} : \mathbf{z}^T(\overline{\mathbf{z}} - \mathbf{z}_0) \leq \frac{1}{\varepsilon} \right\}$. Similarly, we repeat the above procedure to construct a sequential nested polytope for which $\mathcal{B}^{(1)} \supset \mathcal{B}^{(2)} \supset \cdots \supset \mathcal{B}^{(m)} \supset \widetilde{\mathcal{C}}^{\text{o}}$. The proposed SUCM-based placement optimization algorithm is summarized in TABLE I.

With (x_u^*, y_u^*) as given in TABLE I, it can be verified that (20a) is monotonic decreasing in h_u. From (20b), it follows that the optimal flight altitude h_u^* is given by

$$h_u^* = \max \left\{ \frac{\sqrt{Q_{\max}}}{\tan \Theta}, h_{min} \right\}, \tag{29}$$

where $Q_{\max} = \max_{k=1,\cdots,K} \| z_k - z_u \|^2$. Next, we focus on solving the analog beamformer $\{\mathbf{F}\}$ and the digital beamformer $\{\mathbf{W}\}$ with fixed (x_u^*, y_u^*, h_u^*).

B. MOEA/D Based Analog Beamformer Design

The analog beamformer is designed by beam pattern synthesis. The key idea of beam pattern synthesis is to optimize the sidelobe level (SLL), array gain and beamwidth through controlling the phases [9]. Mathematically, this can be tackled by a multiobjective optimization framework

$$\min \ F(\boldsymbol{\vartheta}) = (f_1(\boldsymbol{\vartheta}), f_2(\boldsymbol{\vartheta}), f_3(\boldsymbol{\vartheta}))^T$$

$$\text{s.t. } \boldsymbol{\vartheta} \in \mathbf{R}^{M \times N}, \tag{30}$$

where $f_1(\boldsymbol{\vartheta}) = SLL(\boldsymbol{\vartheta})$, $f_2(\boldsymbol{\vartheta}) = \frac{1}{|\mathbf{E}(\theta,\phi)|}$, and $f_3(\boldsymbol{\vartheta}) = \frac{1}{|\Theta_{h,e}|}$. $\boldsymbol{\vartheta} = [\vartheta_{1n}, \cdots, \vartheta_{mn}, \cdots, \vartheta_{MN}]^T$ denotes the phases of the $M \times N$ antenna array. $SLL(\boldsymbol{\vartheta}) = 20 \log \frac{|\mathrm{AF}_{msl}|}{|\mathrm{AF}_{max}|}$ denotes the SLL of the $M \times N$ antenna array [30], where AF_{msl} and AF_{max} represent the array factor of the maximum SLL and the main-lobe, respectively [9]. Note that the array factor of the $M \times N$ antenna array is $\mathrm{AF} = \sum_{m=1}^{M} \sum_{n=1}^{N} I_{mn} \times e^{j2\pi/\lambda d_{array} \sin(\theta)[(m-1)\cos(\phi)+(n-1)\sin(\phi)]+\vartheta_{mn}}$ [30]. $\mathbf{E}(\theta, \phi) = \mathbf{a}^H(\theta, \phi)\mathbf{F}$ is the synthesized pattern, and $\mathbf{F} = e^{j\boldsymbol{\vartheta}}$. $\Theta_{h,e}$ represents the elevation plane half-power beamwidth. To solve problem (30), a multiobjective evolutionary algorithm (MOEA/D) solution is proposed here. The steps of this algorithm are presented as follows.

- *Input*: Let $\{N_{sub}, \boldsymbol{\beta}^i, S_{nei}, iter\}$ be a set of input parameters. Here, N_{sub} denotes the number of subproblems. $\boldsymbol{\beta}^i = (\beta_1^i, \cdots, \beta_d^i)^T, i = 1, \cdots, N_{sub}, 1 \leq d \leq 3$ is the weight vector of the ith subproblem. S_{nei} represents the number of weight vectors considered to be neighbors of each weight vector and $iter$ is the iteration index.

- *Output*: The output is a non-dominated set ND[2].

- *Initialization*: We first select S_{nei} as the closest weight vectors of $\boldsymbol{\beta}^i$ by calculating the Euclidean distance, whose indices are stored in $\mathcal{C}(i)$. Then, we generate the initial solutions $\boldsymbol{\vartheta}_1, \cdots, \boldsymbol{\vartheta}_{N_{sub}}$ randomly, and then update the F-values $FV_i = F(\boldsymbol{\vartheta}_i)$ and the best-so-far solutions $\mathcal{L} = (L_1, \cdots, L_j, \cdots, L_d)^T$. Here, $L_j = \min\{f_j(\boldsymbol{\vartheta}), \boldsymbol{\vartheta} \in \mathbf{R}^{M \times N}\}$.

- *Update*: For each $i = 1, \cdots, N_{sub}$, we choose two weight vectors $\boldsymbol{\vartheta}_k$ and $\boldsymbol{\vartheta}_l$ from $\mathcal{C}(i)$ and then generate a new solution $\boldsymbol{x}$ by applying the differential evolution (DE) algorithm [32]. Then,

---

[2]Let $\omega, \nu \in \mathbf{R}^n$, ν is dominated by ω if and only if $\omega_i \leq \nu_i, i \in \{1, \cdots, n\}$ and $\omega_j < \nu_j, \exists j \in \{1, \cdots, n\}$ [31].

we update the best-so-far solutions and the F-value of $\boldsymbol{\vartheta}_i$. Specifically, for $j = 1, \cdots, d$, if $L_j > f_j(\boldsymbol{x})$, it follows that $L_j = f_j(\boldsymbol{x})$; if $g^{te}(\boldsymbol{x} \mid \boldsymbol{\beta}^j, \mathcal{L}) \leq g^{te}(\boldsymbol{\vartheta}_j \mid \boldsymbol{\beta}^j, \mathcal{L})$, it follows that $\boldsymbol{\vartheta}_j = \boldsymbol{x}$ and $FV_j = F(\boldsymbol{x})$. Here, $g^{te}(\boldsymbol{x} \mid \boldsymbol{\beta}^j, \mathcal{L}) = \max_{1 \leq t \leq d}\{\beta_t^j | f_t(\boldsymbol{x}) - L_t|\}$ [31]. $F(\boldsymbol{x})$ will be stored in ND if it dominates other weight vectors, and all weight vectors from ND dominated by $F(\boldsymbol{x})$ are eliminated.

- *Stopping*: The algorithm terminates if the iterations have converged; otherwise, go back to *Update*.

The Pareto solutions can be obtained by the MOEA/D based algorithm, whose convergence performance is similar to [31] and thus we omit it here.

C. DDPG Based Digital Beamformer Design

Based on the optimal 3D placement of the UAV and the analog beamformer, it can be verified that constraint (20b) and (20c) are satisfied, and problem (P3) is then rewritten as

$$(\text{P3.3}) : \max_{\mathbf{W}} \ \sum_{k=1}^{K} aT\xi_0 P_0 |\mathbf{h}_k^H \mathbf{F} \mathbf{w}_k|^2 \tag{31a}$$

$$\text{s.t.} \ \sum_{k=1}^{K} \| \mathbf{F}\mathbf{w}_k \|^2 \leq P_{th}, \tag{31b}$$

Problem (P3.3) can be efficiently solved using the semi-definite relaxation (SDR) approach. By introducing $\overline{\mathbf{h}}_k = \mathbf{h}_k^H \mathbf{F}$, $\mathbf{H} = \sum_{k=1}^{K} aT\xi_0 P_0 \overline{\mathbf{h}}_k \overline{\mathbf{h}}_k^H$, $\mathbf{S} = \mathbf{F}\mathbf{F}^H$, $\overline{\mathbf{W}}_k = \mathbf{w}_k \mathbf{w}_k^H$, problem (P3.3) can be relaxed as

$$(\text{P3.4}) : \max_{\overline{\mathbf{W}}_k} \ \sum_{k=1}^{K} \text{tr}(\mathbf{H}\overline{\mathbf{W}}_k) \tag{32a}$$

$$\text{s.t.} \ \sum_{k=1}^{K} \text{tr}(\mathbf{S}\overline{\mathbf{W}}_k) \leq P_{th}, \tag{32b}$$

$$\overline{\mathbf{W}}_k \succeq 0. \tag{32c}$$

Problem (P3.4) is a convex semi-definite programming (SDP) problem, and hence can be tackled by the interior-point methods [25]. However, the interior-point methods have high memory requirements and thus are difficult to implement in large-scale problems, i.e., matrices with large size. Consequently, we propose a learning-based method to optimize the digital beamformer. In this paper, we adopt the deep deterministic policy gradient (DDPG) instead of the deep Q network (DQN) which is due to the fact that DDPG is the only algorithm which can handle continuous value action space and provide a

continuous decision value.

For the considered UAV-aided wireless-powered MEC system, we have obtained the analog beam-forming matrix by the MOEA/D based algorithm, which will act as the basis of our digital precoding matrix design. The DDPG algorithm has three elements, i.e., states, actions and rewards, and the DDPG process can be described as follows

- *Initialization:* Initialize the critic network $Q(s, a|\theta^Q)$ with weights θ^Q and actor network $\mu(s|\theta^\mu)$ with θ^μ. Initialize the target network Q' with weights $\theta^{Q'}$ and target network μ' with $\theta^{\mu'}$, while $\theta^{Q'} = \theta^Q$ and $\theta^{\mu'} = \theta^\mu$. Initialize the replay memory R.

- *Loop:*
  1) Observe the status s_t. The status consists of the distance between the UAV and the IoT devices as well as the unwrapped analog precoding matrix, i.e., $[d_k, real(\mathbf{f}_1), imag(\mathbf{f}_1), \ldots, real(\mathbf{f}_{N_a^t}), imag(\mathbf{f}_{N_a^t})]$.

  2) Generate an action as $a_t = \mu(s_t|\theta^\mu) + \mathcal{N}_t$, where $\mathcal{N}_t$ is an exploration process and t is the iteration index. $\mu(s_t|\theta^\mu)$ is an action generation policy. This exploration process guarantees that the action choice will not fall into a local optimum.

  3) Execute action a_t and calculate the reward r_t, while observing the next time slot status s_{t+1}. Then, put the memory (s_t, a_t, r_t, s_{t+1}) into the replay memory R.

  4) Randomly select a training batch of N from R, that is (s_i, a_i, r_i, s_{i+1}), $i \in \{1, \cdots, N\}$. Set $y_i = r_i + \gamma Q'(s_{i+1}, \mu'(s_{i+1}|\theta^{\mu'})|\theta^{Q'})$ and calculate the result.

  5) Update the critic network and the actor policy by minimizing the loss $L = \frac{1}{N}\sum_i(y_i - Q(s_i, a_i|\theta^Q))^2$ and the gradient $\Delta_{\theta^\mu}\mathcal{J} \approx \frac{1}{N}\sum_i \Delta_a Q(s, a|\theta^Q)|_{s=s_i, a=\mu(s_i)}\Delta_{\theta|mu}\mu(s|\theta^\mu)|_{s_i}$, respectively. Update the target network weights as $\theta^{Q'} \leftarrow \tau\theta^Q + (1-\tau)\theta^{Q'}$ and $\theta^{\mu'} \leftarrow \tau\theta^\mu + (1-\tau)\theta^{\mu'}$.

- *Stopping:* The algorithm terminates if the loop process reaches a predetermined number.

- *Output:* The digital precoding matrix.

IV. NOMA-BASED RESOURCE ALLOCATION ALGORITHM IN PARTIAL OFFLOADING MODE

In this section, a NOMA-based resource allocation algorithm in partial offloading mode is proposed, where the WPT time allocation a, the transmit power of IoT devices P_k, the computation time of IoT devices t_k and the CPU frequencies f_k are jointly optimized in an iterative manner.

With solved (x_u^*, y_u^*, h_u^*), $\mathbf{F}^*$ and $\mathbf{W}^*$, problem (P1) is expressed as

$$(\text{P4}): \max_{a, P_k, t_k, f_k} \sum_{k=1}^{K} \left[\frac{f_k t_k}{CT} + B(1-a) \log_2 \left(1 + \frac{P_k g_k}{\sum_{i=k+1}^{K} P_i g_i + N_0} \right) \right] \tag{33a}$$

$$\text{s.t. } \tau_k f_k^3 t_k + P_k(1-a)T \le aT\xi_0 P_0 |\mathbf{h}_k^H \mathbf{F} \mathbf{w}_k|^2, k \in \mathcal{M}, \tag{33b}$$

$$0 \le t_k \le T, \tag{33c}$$

$$0 \le a \le 1, \tag{33d}$$

$$P_k \ge 0, \tag{33e}$$

$$0 \le f_k \le f_{max}. \tag{33f}$$

Problem (P4) is non-convex. To tackle this problem, the considered problem is decoupled into two subproblems. Particularly, for given a and t_k, problem (P4) is written as

$$(\text{P4.1}): \max_{P_k, f_k} \sum_{k=1}^{K} \left[\frac{f_k t_k}{CT} + B(1-a) \log_2 \left(1 + \frac{P_k g_k}{\sum_{i=k+1}^{K} P_i g_i + N_0} \right) \right] \tag{34a}$$

$$\text{s.t. } \tau_k f_k^3 t_k + P_k(1-a)T \le aT\xi_0 P_0 |\mathbf{h}_k^H \mathbf{F} \mathbf{w}_k|^2, k \in \mathcal{M}, \tag{34b}$$

$$P_k \ge 0, \tag{34c}$$

$$0 \le f_k \le f_{max}. \tag{34d}$$

Problem (4.1) is still a non-convex problem due to the second term of (34a). By applying the logarithmic transformation, we transform $\sum_{k=1}^{K} B(1-a) \log_2 \left(1 + \frac{P_k g_k}{\sum_{i=k+1}^{K} P_i g_i + N_0} \right)$ as

$$B(1-a) \log_2 \left(\frac{\sum_{i=1}^{K} P_i g_i + N_0}{N_0} \right). \tag{35}$$

Using (35), (P4.1) is expressed as the following equivalent problem

$$(\text{P4.2}): \max_{P_k, f_k} \sum_{k=1}^{K} \frac{f_k t_k}{CT} + B(1-a) \log_2 \left(\frac{\sum_{i=1}^{K} P_i g_i + N_0}{N_0} \right) \tag{36a}$$

$$\text{s.t. } \tau_k f_k^3 t_k + P_k(1-a)T \le aT\xi_0 P_0 |\mathbf{h}_k^H \mathbf{F} \mathbf{w}_k|^2, k \in \mathcal{M}, \tag{36b}$$

$$P_k \ge 0, \tag{36c}$$

$$0 \le f_k \le f_{max}. \tag{36d}$$

For the objective function given by (36a), $\frac{f_k t_k}{CT}$ is a linear function of the CPU frequency f_k and $B(1-a) \log_2 \left(\frac{\sum_{i=1}^{K} P_i g_i + N_0}{N_0} \right)$ is concave with respect to P_i. For the constraint $\tau_k f_k^3 t_k + P_k(1-a)T \le$

$aT\xi_0 P_0|\mathbf{h}_k^H\mathbf{F}\mathbf{w}_k|^2$, the right side $aT\xi_0 P_0|\mathbf{h}_k^H\mathbf{F}\mathbf{w}_k|^2$ is a constant and the left side $\tau_k f_k^3 t_k + P_k(1-a)T$ is a convex function with respect to f_k and a linear function in regard to P_k. Moreover, the constraints (36c) and (36d) are linear inequality constraints. Thus, problem (P4.2) is a convex optimization problem and can be tackled using convex optimization methods [33]. Next, the Lagrange duality method is applied to achieve the closed-form solutions of the CPU frequencies and the UAV's transmit power for offloading.

Proposition 2: For given WPT time allocation a and computation time t_k, the optimal solution of problem (P4.2) can be given by

$$f_k^* = \sqrt{\frac{1}{3\lambda_k \tau_k CT}}, \tag{37}$$

$$\sum_{m=k}^{K} P_m^* g_m = \left[\frac{Bg_k}{\lambda_k T \ln 2} - N_0\right]^+, \tag{38}$$

where $[x]^+$ denotes $\max(x, 0)$.

Proof: Please refer to Appendix A for the proof of Proposition 2. ∎

To obtain the optimal solution of problem (P4.2), we adopt the subgradient approach where the dual variables are updated through iteration process [34]. Therefore, in the $(n+1)$th iteration, the dual variable $\lambda_k(n+1)$ is given by

$$\lambda_k(n+1) = [\lambda_k(n) - \delta\Delta\lambda_k(n)]^+, \tag{44}$$

where δ represents a sufficiently small positive step-size. $\Delta\lambda_k(n)$ is the corresponding subgradient that is expressed as

$$\Delta\lambda_k(n) = aT\xi_0 P_0|\mathbf{h}_k^H\mathbf{F}\mathbf{w}_k|^2 - \tau_k f_k^3 t_k - P_k(1-a)T. \tag{45}$$

For a given CPU frequency f_k^* and transmit power for offloading P_k^*, problem (P4) is rewritten as

$$(\text{P4.3}) : \max_{a, t_k} \sum_{k=1}^{K}\left[\frac{f_k t_k}{CT} + B(1-a)\log_2\left(1 + \frac{P_k g_k}{\sum_{i=k+1}^{K} P_i g_i + N_0}\right)\right] \tag{46a}$$

$$\text{s.t.} \quad \tau_k f_k^3 t_k + P_k(1-a)T \le aT\xi_0 P_0|\mathbf{h}_k^H\mathbf{F}\mathbf{w}_k|^2, k \in \mathcal{M}, \tag{46b}$$

$$0 \le t_k \le T, \tag{46c}$$

$$0 \le a \le 1. \tag{46d}$$

Since the objective function and constraints are linear functions with respect to a and t_k, problem (P4.3) is a linear programming problem. Thus, problem (P4.3) can be tackled effectively through the

TABLE II: THE RESOURCE ALLOCATION ALGORITHM FOR PARTIAL OFFLOADING MODE

1: Initialize $(\lambda_k(n), f_k(n), P_k(n), a(n), P_k(n))$;
   Iterate index: n=1;
2: **ITERATE**
   $\rhd$ For given $a^*(n), t_k^*(n)$, obtain $\lambda_k(n)$ by (44),
      then calculate $f_k^*(n)$ and $P_k^*(n)$ by (37) and (38);
   $\rhd$ For given $f_k^*(n), P_k^*(n)$, solve (P4.3) by CVX,
      then calculate $a^*(n)$ and $t_k^*(n)$;
   $\rhd$ Set $n \leftarrow n + 1$;
3: **UNTIL: CONVERGENCE**;
4: **OUTPUT:**
   $f_k^* = f_k^*(n), P_k^* = P_k^*(n), a^* = a^*(n), t_k^* = t_k^*(n)$.

CVX toolbox [35].

The resource allocation algorithm for tackling problem (P4) is summarized in TABLE II. In each iteration, (36a) is maximized over (f_k, P_k), while keeping (a, t_k)'s fixed. For a given (f_k, P_k), the set of (a, t_k) is obtained via solving problem (P4.3). The algorithm terminates if it converges to a fixed point.

V. NOMA-Based Resource Allocation algorithm in Binary Offloading Mode

In this section, a resource allocation algorithm in binary offloading pattern is studied under given mode selection. Then, a channel-gain-based mode selection method is proposed to optimize the model selection.

A. Resource Allocation Under Given Mode Selection

For given α_k, (x_u^*, y_u^*, h_u^*), $\mathbf{F}^*$ and $\mathbf{W}^*$, problem (P2) is formulated as

$$(\text{P5}) : \max_{a, P_j, t_k, f_k} \sum_{k \in \mathcal{M}_0} \frac{f_k t_k}{CT} + \sum_{j \in \mathcal{M}_1} B(1-a) \log_2 \left(1 + \frac{P_j g_j}{\sum_{i=j+1}^K P_i g_i + N_0} \right) \tag{47a}$$

$$\text{s.t. } \tau_k f_k^3 t_k \leq aT\xi_0 P_0 |\mathbf{h}_k^H \mathbf{F} \mathbf{w}_k|^2, k \in \mathcal{M}_0, \tag{47b}$$

$$P_j(1-a)T \leq aT\xi_0 P_0 |\mathbf{h}_j^H \mathbf{F} \mathbf{w}_j|^2, j \in \mathcal{M}_1, \tag{47c}$$

$$0 \leq t_k \leq T, k \in \mathcal{M}_0, \tag{47d}$$

$$0 \leq a \leq 1, \tag{47e}$$

$$P_j \geq 0, j \in \mathcal{M}_1, \tag{47f}$$

$$0 \le f_k \le f_{max}, k \in \mathcal{M}_0. \tag{47g}$$

Similar to (18), problem (P5) is a mixed combinatorial non-convex problem. Note that when the WPT time a is fixed, the CPU frequency f_k and the computation time t_k of each device k ($k \in \mathcal{M}_0$) can be optimized independently without affecting the computation performance of other IoT devices. Moreover, the maximum local computation rate can be obtained by optimizing f_k and t_k. Motivated by this, we then have the following proposition.

Proposition 3: The optimal CPU frequencies and the computation time to maximize the local computation rate subject to the energy harvesting constraint are given by

$$t_k^* = T, \ f_k^* = \left(\frac{a\xi_0 P_0 |\mathbf{h}_k^H \mathbf{F} \mathbf{w}_k|^2}{\tau_k} \right)^{\frac{1}{3}}, \forall k \in \mathcal{M}_0. \tag{48}$$

Proof: Please refer to Appendix B for the proof of Proposition 3. ∎

With t_k^* and f_k^* given in (48) and by substituting (35) into problem (P5), problem (P5) is equivalently expressed as

$$(\text{P5.1}) : \max_{a, P_j} \sum_{k \in \mathcal{M}_0} a^{\frac{1}{3}} \left(\frac{\xi_0 P_0 |\mathbf{h}_k^H \mathbf{F} \mathbf{w}_k|^2}{\tau_k} \right)^{\frac{1}{3}} \frac{1}{C} + B(1-a) \log_2 \left(1 + \frac{\sum_{i=1}^{l_1} P_i g_i}{N_0} \right) \tag{49a}$$

$$\text{s.t. } P_j(1-a)T \le aT\xi_0 P_0 |\mathbf{h}_j^H \mathbf{F} \mathbf{w}_j|^2, j \in \mathcal{M}_1, \tag{49b}$$

$$0 \le a \le 1, \tag{49c}$$

$$P_j \ge 0, j \in \mathcal{M}_1. \tag{49d}$$

It can be observed from problem (P5.1) that as the transmission power of the IoT devices P_j increases, so does the sum computation rate. Therefore, the optimal transmission power P_j should be as large as possible within the range of its energy harvesting $aT\xi_0 P_0 |\mathbf{h}_j^H \mathbf{F} \mathbf{w}_j|^2$, which can be achieved based on (49b) and is given by

$$P_j^* = \frac{a\xi_0 P_0 |\mathbf{h}_j^H \mathbf{F} \mathbf{w}_j|^2}{1-a}, j \in \mathcal{M}_1. \tag{50}$$

From (50), it is observed that the transmission power of the IoT devices depends on the WPT time allocation a. Using (50), the optimal WPT time a^* can be achieved by considering the following equivalent problem (P5.2) derived from problem (P5.1):

$$(\text{P5.2}) : \max_{a} \sum_{k \in \mathcal{M}_0} a^{\frac{1}{3}} \left(\frac{\xi_0 P_0 |\mathbf{h}_k^H \mathbf{F} \mathbf{w}_k|^2}{\tau_k} \right)^{\frac{1}{3}} \frac{1}{C} + B(1-a) \log_2 \left(1 + \frac{\gamma a}{1-a} \right) \tag{51a}$$

TABLE III: THE CHANNEL-GAIN-BASED MODE SELECTION ALGORITHM

```
1: Initialize $g_k, \forall k \in \mathcal{M}$, $\mathbf{D}_{sort} \leftarrow sort(g_k)$ , $m = 0$;
2: REPEAT:
       IF $m = 0$
         $\mathcal{M}_1 \leftarrow \{\emptyset\}$;
       ELSE
         $\mathcal{M}_1 \leftarrow \{1, \cdots, m\}$;
       END
       Obtain optimal $a_m^*$ and $R_{sum}^m$ using the Bisection method
       under $\mathcal{M}_1$ and $\mathbf{D}_{sort}$; Set $m \leftarrow m + 1$;
3: UNTIL: $m = K$;
4: OUTPUT:
       $R_{sum}^{max} \leftarrow \max(R_{sum}^m)$, $\mathcal{M}_1$.
```

$$\text{s.t. } 0 \le a \le 1, \tag{51b}$$

where $\gamma = \sum_{i=1}^{l_1} \frac{\xi_0 P_0 |\mathbf{h}_i^H \mathbf{F} \mathbf{w}_i|^2 g_i}{N_0}$. From (51a), the left side $\sum_{k \in \mathcal{M}_0} a^{\frac{1}{3}} \left(\frac{\xi_0 P_0 |\mathbf{h}_k^H \mathbf{F} \mathbf{w}_k|^2}{\tau_k} \right)^{\frac{1}{3}} \frac{1}{C}$ is a concave function with respect to a. The right side $B(1 - a) \log_2 \left(1 + \frac{\gamma a}{1-a} \right)$ is also a concave function with respect to a. Thus, problem (P5.2) is a convex optimization problem. Denote $q(a)$ as the first-order derivative of a, which is defined as

$$q(a) = \frac{1}{3} a^{-\frac{2}{3}} \sum_{k \in \mathcal{M}_0} \left(\frac{\xi_0 P_0 |\mathbf{h}_k^H \mathbf{F} \mathbf{w}_k|^2}{\tau_k} \right)^{\frac{1}{3}} \frac{1}{C}$$
$$+ B \left(\frac{(1 - a)(\gamma - 1)}{\ln 2[(\gamma - 1)a + 1]} - \log_2 \left(\frac{(\gamma - 1)a + 1}{1 - a} \right) + \frac{1}{\ln 2} \right). \tag{52}$$

Given the concavity of the above problem (P5.2), the optimal WPT time a^* can be achieved at $q(a^*) = 0$. To facilitate the solution, the bisection method is applied to find a^*. Note that when the optimal WPT time allocation a^* in problem (P5.2) is obtained, the corresponding transmission power P_j^* is then achieved.

B. Channel-Gain-Based Mode Selection Optimization

In this subsection, we study the offloading decision of task execution between local execution and task offloading. Since it is hard to jointly optimize K binary variables α_k, an effective algorithm is proposed here. From (35), the achievable transmission rate of IoT devices is independent of the decoding order [36]. Thus, the sum computation rate of all IoT devices is not affected by the NOMA decoding when the set of IoT devices operated in task offloading $\mathcal{M}_1$ and the WPT time allocation a

TABLE IV: PARAMETERS SETTINGS

Parameters	Notation	Values
The channel power gain	β_0	-20 dB
The path loss factor	α	2
The energy conversion efficiency	ξ_0	0.8
The transmit power of UAV	P_0	3 W
The communication bandwidth	B	20 MHz
The noise power	N_0	10^{-9} W
The number of cycles for one bit	C	200 cycles/bit
The capacitance coefficient	τ_k	10^{-26}
The whole period	T	1 s
The minimum altitude of UAV	h_{min}	5 m
The maximum altitude of UAV	h_{max}	21 m
The effective illumination angle	2Θ	$80°$

are given. Motivated by this, we propose the channel-gain-based mode selection scheme to determine $\mathcal{M}_1$ by considering the channel characteristics of the UAV-ground links. First, based on the channel power gain $g_k, \forall k \in \mathcal{M}$, all IoT devices are ranked in a descending order. Subsequently, the objective value R_{sum} of problem (P5.2) and the WPT time allocation a are obtained by considering $\mathcal{M}_1 = \{\emptyset\}$ and $\mathcal{M}_1 = \{1, \cdots, m\}, m = 1, \cdots, K$. Finally, the computing mode with the maximum objective value is chosen. The algorithm is outlined in TABLE III.

Remark 1: The complexity of ordering the IoT devices is $\mathcal{O}(K \log_2(K))$. Furthermore, the complexity of the bisection approach with precision parameter σ_0 is $\mathcal{O}(\log_2(1/\sigma_0))$. To sum up, the complexity of the channel-gain-based mode selection algorithm is then $\mathcal{O}(K \log_2(K/\sigma_0))$.

VI. SIMULATION RESULTS

We provide numerical results to validate the performance of all presented algorithms. For convenience, we assume that the UAV-carried wireless-powered MEC network has $K = 4$ IoT devices, whose positions are $(10, 10)$, $(0, 10)$, $(10, 0)$ and $(0, 0)$, respectively. It is assumed that the 8×8 UAV-mounted antenna array is separated into four 4×4 rectangular arrays. The parameter settings for the resource allocation schemes are similar in [2], [9], [16], and the details of parameter settings are presented in TABLE IV. It should be noted that these parameters settings are selected to illustrate the performance in an example and can be changed to any other values relying on the specific scenario under consideration.

First, we compare the beam pattern response of our designed hybrid beamforming with that of the analog beamforming recently designed in [9]. It is assumed that the excitation amplitude and element
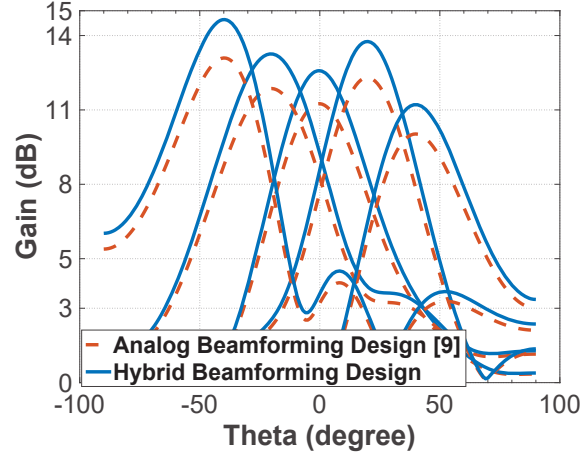
Fig. 4: An example of the beam pattern response for the hybrid beamforming design with $\phi = 90°$.
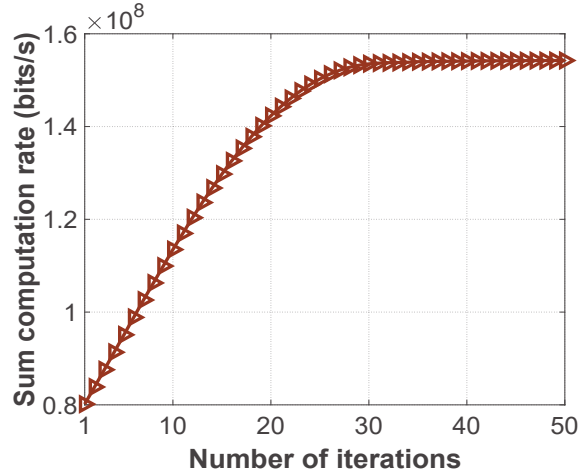

Fig. 5: An example of the convergence behavior of the resource allocation algorithm for the partial offloading mode in a multiuser UAV-aided wireless powered MEC system.

spacing of the antenna array are 1 A and 5.5 mm. The beam directions are $(-40°, 90°)$, $(-20°, 90°)$, $(0°, 0°)$, $(20°, 90°)$ and $(40°, 90°)$. It is observed in Fig. 4 that the main lobe responses achieved by our proposed hybrid beamforming outperforms the analog beamforming. This is due to the fact that when the analog beamforming is determined, the digital beamforming weights can be optimized to further improve the gain. Furthermore, the main-lobe gain of our proposed scheme is 8 dB more than the gain of sidelobes.

Next, we investigate the convergence behavior of the resource allocation algorithm for solving problem (P4). We set $P_0 = 1$ and $K = 4$. The convergence behavior of the proposed algorithm is characterized by illustrating how the sum computation rate behaves with iteration times. As seen in
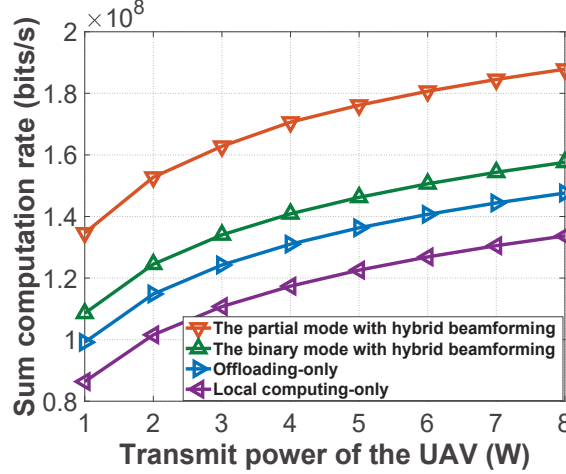
Fig. 6: The sum computation rate of all IoT devices versus the transmit power of the UAV under different resource allocation schemes.

Fig. 5, since the proposed resource allocation algorithm for the partial offloading mode involves a joint WPT time allocation and computation resource scheduling procedure, the sum computation rate converges to a fixed value after around 28 iterations.

We then show the sum computation rate of the two resource allocation algorithms under partial offloading pattern and binary offloading pattern, and compare them to the "offloading-only" scheme and the "local computing-only" scheme. The number of IoT devices is fixed to $K = 4$, while the transmit power of the UAV varies from 1 W to 8 W. As shown in Fig. 6, the resource allocation algorithm under the partial offloading pattern achieves a high sum computation rate compared to the binary offloading mode. This is because all the IoT devices can flexibly choose the computing mode depending on their channel conditions in the partial offloading pattern, whilst the computation task is implemented either locally at the IoT devices or at the UAV in the binary offloading mode. Moreover, the "offloading-only" scheme can achieve higher performance compared with the "local computing-only" scheme when the transmit power becomes large.

In the next simulation, we investigate the sum computation rate for both partial and binary offloading patterns with different transmit powers. To show the computation performance, we compare with the "CD" algorithm in [2] and the "joint optimization" algorithm in [16]. We assume that there are $K = 4$ IoT devices and $P_0 = 1$. From Fig. 7, it can be seen that the sum computation rates achieved by our two proposed resource allocation algorithms outperform both the "CD" algorithm and the "joint optimization" algorithm. This is due to the fact that both the "CD" algorithm and the "joint optimization" algorithm only use a single antenna for WPT. In particular, our proposed
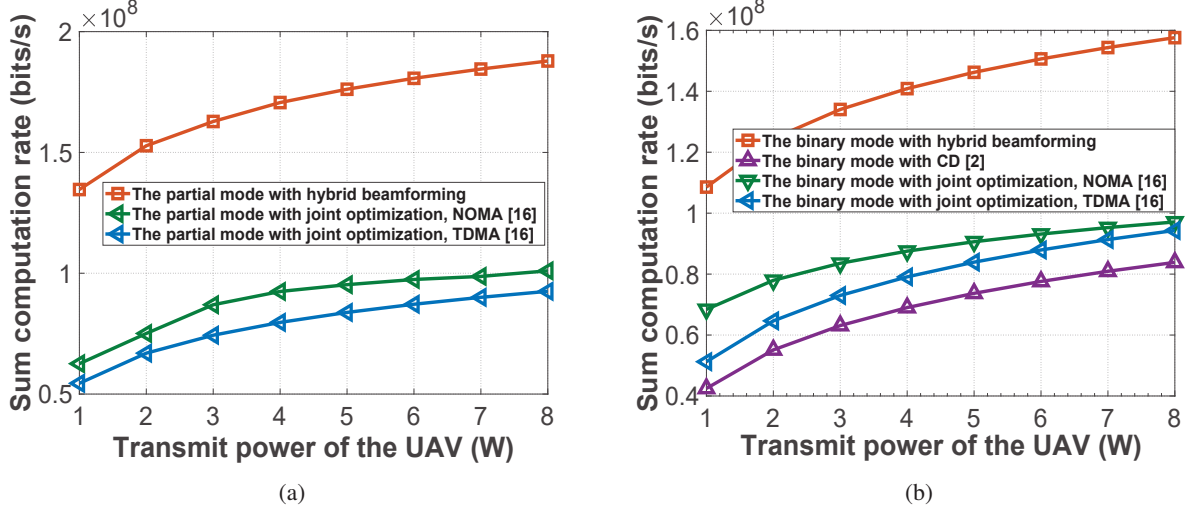
Fig. 7: The performance of two proposed resource allocation algorithms: (a) The sum computation rate versus the transmit power of the UAV under the partial offloading mode; (b) The sum computation rate versus the transmit power of the UAV under the binary offloading mode.

resource allocation algorithms enable the UAV-mounted antenna array to form multiple beams to charge IoT devices which can compensate for the high propagation loss, which thereby improves the sum computation rate. Moreover, our proposed algorithms employ NOMA which enables multiple IoT devices to transmit their tasks to the UAV simultaneously, and thus improve the performance in terms of the sum computation rate.

We then study the sum computation rate of the two proposed resource allocation algorithms under different number of IoT devices. In Fig. 8, the sum computation rate achieved by the two resource allocation algorithms are monotonically non-decreasing with the number of IoT devices. Particularly, the sum computation rate increases with a small quantity of IoT devices, i.e., $K < 3$, and then saturates when $K \geq 3$. This is because the interference is also increasing with the growing number of IoT devices, and the sum computation rate is still limited in this case.

Finally, we investigate the sum computation rate versus the minimum altitude of the UAV for the two resource allocation algorithms. As shown in Fig. 9, both resource allocation algorithms achieve good performance with a lower minimum altitude, i.e., $h_{min} \leq 10$, but achieve poor performance when $h_{min} > 10$. This is due to the fact that increasing the minimum altitude of the UAV will degrade the channel quality of IoT devices, and thus restrict the improvement of the sum computation rate.
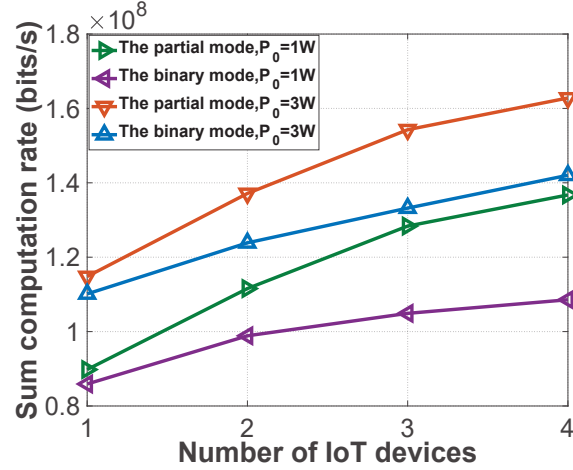
Fig. 8: The sum computation rate of all IoT devices versus the number of IoT devices under different resource allocation schemes.
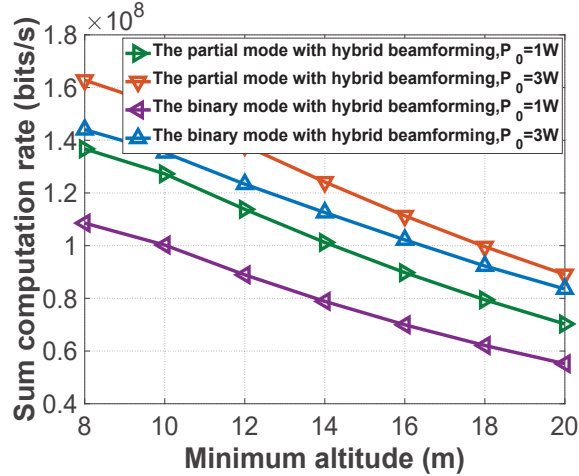

Fig. 9: The sum computation rate of all IoT devices versus the minimum altitude of the UAV under different resource allocation schemes.

VII. CONCLUSION

This paper exploited hybrid beamforming and NOMA for enhancing the computation performance of UAV-aided wireless-powered MEC networks. By considering both partial and binary offloading patterns, we maximized the sum computation rate at all the IoT devices by jointly optimizing the UAV's 3D position, hybrid beamforming design and computation resource allocation. To tackle these problems, we first presented a SUCM-based placement optimization algorithm to derive the closed-form solution of the 3D placement of the UAV. Subsequently, a learning-based two-stage hybrid beamforming algorithm was proposed for beamforming design. Furthermore, two resource allocation algorithms for

two computing modes were then presented to maximize the sum computation rate. Numerical results demonstrated that the sum computation rate of all the IoT devices can be significantly enhanced by the designed resource allocation algorithms compared to the benchmark schemes.

APPENDIX A

PROOF OF PROPOSITION 2

By adding a set of non-negative dual variables, λ_k, $k = 1, \cdots, K$, associated with the energy harvesting constraints for the IoT devices in problem (P4.2), the Lagrangian function of problem (P4.2) can be expressed as

$$L(\lambda_k, f_k, P_k) = \sum_{k=1}^{K} \frac{f_k t_k}{C_k T} + B(1-a) \log_2 \left(\frac{\sum_{i=1}^{K} P_i g_i + N_0}{N_0} \right)$$

$$+ \sum_{k=1}^{K} \lambda_k \left[aT\xi_0 P_0 |\mathbf{h}_k^H \mathbf{F} \mathbf{w}_k|^2 - \tau_k f_k^3 t_k - P_k(1-a)T \right]. \tag{39}$$

Then, the derivatives of $L(\lambda_k, f_k, P_k)$ with respect to f_k and P_k are given by

$$\frac{\partial L(\lambda_k, f_k, P_k)}{\partial f_k} = \frac{t_k}{C_k T} - 3\lambda_k \tau_k f_k^2 t_k, \tag{40}$$

$$\frac{\partial L(\lambda_k, f_k, P_k)}{\partial P_k} = \frac{B(1-a)g_k}{(\sum_{m=k}^{K} P_m g_m + N_0) \ln 2} - (1-a)T. \tag{41}$$

By applying the Karush-Kuhn-Tucher (KKT) conditions [33], we can obtain the optimal solutions of problem (P4.2)

$$f_k^* = \sqrt{\frac{1}{3\lambda_k \tau_k C_k T}}, \tag{42}$$

$$\sum_{m=k}^{K} P_m^* g_m = \left[\frac{Bg_k}{\lambda_k T \ln 2} - N_0 \right]^+. \tag{43}$$

Therefore, this completes the proof of Proposition 2.

APPENDIX B

PROOF OF PROPOSITION 3

Since the local computation rate of IoT devices $r_{L,k}^{bin}$ is increasing with respect to t_k and f_k, the maximum $r_{L,k}^{bin}$ can be obtained from (47a) with $t_k^* = T$. This implies that the devices compute during the whole period T. Substituting $t_k^* = T$ into (47b) and applying $0 \le f_k \le f_{max}$ yields the following

optimal CPU frequency as $f_k^* = \min\left(\left(\frac{a\xi_0 P_0 |\mathbf{h}_k^H \mathbf{F}\mathbf{w}_k|^2}{\tau_k}\right)^{\frac{1}{3}}, f_{max}\right)$. By combining this result with (12), we finally obtain $f_k^* = \left(\frac{a\xi_0 P_0 |\mathbf{h}_k^H \mathbf{F}\mathbf{w}_k|^2}{\tau_k}\right)^{\frac{1}{3}}$. Therefore, this completes the proof of Proposition 3.

REFERENCES

[1] Z. Liang, Y. Liu, T. Lok, and K. Huang, "Multiuser computation offloading and downloading for edge computing with virtualization," *IEEE Trans. Wireless Commun.*, vol. 18, no. 9, pp. 4298–4311, Sep. 2019.

[2] S. Bi and Y. J. Zhang, "Computation rate maximization for wireless powered mobile-edge computing with binary computation offloading," *IEEE Trans. Wireless Commun.*, vol. 17, no. 6, pp. 4177–4190, Jun. 2018.

[3] M. Liu and Y. Liu, "Price-based distributed offloading for mobile-edge computing with computation capacity constraints," *IEEE Wireless Commun. Lett.*, vol. 7, no. 3, pp. 420–423, Jun. 2018.

[4] W. Feng, J. Tang, Y. Yu, J. Song, N. Zhao, G. Chen, K.-K. Wong, and J. Chambers, "UAV-enabled SWIPT in IoT networks for emergency communications," *IEEE Wireless Commun.*, to be published, DOI: 10.1109/MWC.001.1900656.

[5] Z. Ding, X. Lei, G.K. Karagiannidis, R. Schober, J. Yuan, and V.K. Bhargava, "A survey on non-orthogonal multiple access for 5G networks: Research challenges and future trends," *IEEE J. Sel. Areas Commun.*, vol. 35, no. 10, pp. 2181–2195, Oct. 2017.

[6] F. Wang, J. Xu, and Z. Ding, "Multi-antenna NOMA for computation offloading in multiuser mobile edge computing systems," *IEEE Trans. Commun.*, vol. 67, no. 3, pp. 2450–2463, Mar. 2019.

[7] Z. Yang, C. Pan, J. Hou, and M. Shikh-Bahaei, "Efficient resource allocation for mobile-edge computing networks with NOMA: Completion time and energy minimization," *IEEE Trans. Commun.*, vol. 67, no. 11, pp. 7771–7784, Nov. 2019.

[8] Y. Ye, L. Shi, H. Sun, R. Q. Hu, and G. Lu, "System-centric computation energy efficiency for distributed NOMA-based MEC networks," *IEEE Trans. Veh. Technol.*, vol. 69, no. 8, pp. 8938–8948, Aug. 2020.

[9] W. Feng, N. Zhao, S. Ao, J. Tang, X. Zhang, Y. Fu, D.K.C. So, and K.-K. Wong, "Joint 3D trajectory design and time allocation for UAV-enabled wireless power transfer networks," *IEEE Trans. Veh. Technol.*, to be published, DOI: 10.1109/TVT.2020.2972133.

[10] T. Zhang, Y. Xu, J. Loo, D. Yang, and L. Xiao, "Joint computation and communication design for UAV-assisted mobile edge computing in IoT," *IEEE Trans. Ind. Informat.*, vol. 16, no. 8, pp. 5505–5516, Aug. 2020.

[11] Q. Hu, Y. Cai, G. Yu, Z. Qin, M. Zhao, and G. Y. Li, "Joint offloading and trajectory design for UAV-enabled mobile edge computing systems," *IEEE Internet Things J.*, vol. 6, no. 2, pp. 1879–1892, Apr. 2019.

[12] J. Hu, M. Jiang, Q. Zhang, Q. Li, and J. Qin, "Joint optimization of uav position, time slot allocation, and computation task partition in multiuser aerial mobile-edge computing systems," *IEEE Trans. Veh. Technol.*, vol. 68, no. 7, pp. 7231–7235, Jul. 2019.

[13] Y. Wang, Z. Ru, K. Wang, and P. Huang, "Joint deployment and task scheduling optimization for large-scale mobile users in multi-UAV-enabled mobile edge computing," *IEEE Trans. Cybern.*, vol. 50, no. 9, pp. 3984–3997, Sep. 2020.

[14] J. Tang, A. Shojaeifard, D. K. C. So, K. Wong, and N. Zhao, "Energy efficiency optimization for CoMP-SWIPT heterogeneous networks," *IEEE Trans. Commun.*, vol. 66, no. 12, pp. 6368–6383, Dec. 2018.

[15] J. Tang, D. K. C. So, N. Zhao, A. Shojaeifard, and K. Wong, "Energy efficiency optimization with SWIPT in MIMO broadcast channels for Internet of Things," *IEEE Internet Things J.*, vol. 5, no. 4, pp. 2605–2619, Aug. 2018.

[16] F. Zhou, Y. Wu, R. Q. Hu, and Y. Qian, "Computation rate maximization in UAV-enabled wireless-powered mobile-edge computing systems," *IEEE J. Sel. Areas Commun.*, vol. 36, no. 9, pp. 1927–1941, Sep. 2018.

[17] F. Zhou and R. Q. Hu, "Computation efficiency maximization in wireless-powered mobile edge computing networks," *IEEE Trans. Wireless Commun.*, vol. 19, no. 5, pp. 3170–3184, May 2020.

[18] Y. Liu, K. Xiong, Q. Ni, P. Fan, and K. B. Letaief, "UAV-assisted wireless powered cooperative mobile edge computing: Joint offloading, CPU control, and trajectory optimization," *IEEE Internet Things J.*, vol. 7, no. 4, pp. 2777–2790, Apr. 2020.

[19] F. Wang, J. Xu, and S. Cui, "Optimal energy allocation and task offloading policy for wireless powered mobile edge computing systems," *IEEE Trans. Wireless Commun.*, vol. 19, no. 4, pp. 2443–2459, Apr. 2020.

[20] J. Du, W. Xu, Y. Deng, A. Nallanathan, and L. Vandendorpe, "Energy-saving UAV-assisted multiuser communications with massive MIMO hybrid beamforming," *IEEE Commun. Lett.*, vol. 24, no. 5, pp. 1100–1104, May 2020.

[21] I. Ahmed, H. Khammari, A. Shahid, A. Musa, K. S. Kim, E. De Poorter, and I. Moerman, "A survey on hybrid beamforming techniques in 5G: Architecture and system model perspectives," *IEEE Commun. Surveys Tuts.*, vol. 20, no. 4, pp. 3060–3097, 4th Quart., 2018.

[22] Y. Sun, D. W. K. Ng, Z. Ding, and R. Schober, "Optimal joint power and subcarrier allocation for full-duplex multicarrier non-orthogonal multiple access systems," *IEEE Trans. Commun.*, vol. 65, no. 3, pp. 1077–1091, Mar. 2017.

[23] Z. Wei, L. Yang, D. W. K. Ng, J. Yuan, and L. Hanzo, "On the performance gain of NOMA over OMA in uplink communication systems," *IEEE Trans. Commun.*, vol. 68, no. 1, pp. 536–568, Jan. 2020.

[24] Y. Pochet and L. A. Wolsey, *Production planning by mixed integer programming*, Berlin, Germany: Springer, 2006.

[25] S. Boyd and L. Vandenberghe, *Convex Optimization*. Cambridge, U.K.: Cambridge Univ. Press, 2004.

[26] H. Tuy and F. A. Al-Khayyal, "Global optimization of a nonconvex single facility location problem by sequential unconstrained convex minimization," *J. Global Optim.*, vol. 2, no. 1, pp. 61–71, Mar. 1992.

[27] I. Tsevendorj, "Piecewise-convex maximization problems," *J. Global Optim.*, vol. 21, no. 1, pp. 1–14, Sep. 2001.

[28] J. Borwein and A. S. Lewis, *Convex Analysis and Nonlinear Optimization: Theory and Examples*. New York, NY, USA: Springer-Verlag, 2006.

[29] J. Xu and R. Zhang, "A general design framework for MIMO wireless energy transfer with limited feedback," *IEEE Trans. Signal Process.*, vol. 64, no. 10, pp. 2475–2488, May. 2016.

[30] C. A. Balanis, *Antenna Theory: Analysis and Design*. New York, NY, USA: Wiley, 2016.

[31] Q. Zhang and H. Li, "MOEA/D: A multi-objective evolutionary algorithm based on decomposition," *IEEE Trans. Evol. Comput.*, vol. 11, no. 6, pp. 712–731, Dec. 2007.

[32] R. Storn and K. Price, "Differential evolution: A simple and efficient heuristic for global optimization over continuous spaces," *J. Global Optimization*, vol. 11, no. 4, pp. 341–359, Dec. 1997.

[33] S. Boyd and L. Vandenberghe, *Convex Optimization*. Cambridge, U.K.: Cambridge Univ. Press, 2004.

[34] D. P. Palomar and M. Chiang, "A tutorial on decomposition methods for network utility maximization," *IEEE J. Sel. Areas Commun.*, vol. 24, no. 8, pp. 1439–1451, Aug. 2006.

[35] M. Grant and S. Boyd, "CVX: Matlab software for disciplined convex programming, version 2.2," Jan. 2020 [Online]. Available: http://cvxr.com/cvx.

[36] P. D. Diamantoulakis, K. N. Pappi, Z. Ding, and G. K. Karagiannidis, "Wireless-powered communications with non-orthogonal multiple access," *IEEE Trans. Wireless Commun.*, vol. 15, no. 12, pp. 8422–8436, Dec. 2016.

Hybrid Beamforming Design and Resource Allocation for UAV-aided Wireless-Powered Mobile Edge Computing Networks with NOMA

Wanmei Feng, Jie Tang, *Senior Member, IEEE*, Nan Zhao, *Senior Member, IEEE*,
Xiuyin Zhang, *Senior Member, IEEE*, Xianbin Wang, *Fellow, IEEE*,
Kai-Kit Wong, *Fellow, IEEE* and Jonathon Chambers, *Fellow, IEEE*

Abstract—Beamforming and non-orthogonal multiple access (NOMA) serve as two potential solutions for achieving spectral efficient communication in the fifth generation and beyond wireless networks. In this paper, we jointly apply a hybrid beamforming and NOMA techniques to an unmanned aerial vehicle (UAV)-carried wireless-powered mobile edge computing (MEC) system, within which the UAV is equipped with a wireless power charger and the MEC platform delivers energy and computing services to Internet of Things (IoT) devices. Our aim is to maximize the sum computation rate at all IoT devices whilst satisfying the constraint of energy harvesting and coverage. The resultant optimization problem is non-convex involving joint optimization of the UAV's 3D placement and hybrid beamforming matrices as well as computation resource allocation in both partial and binary offloading patterns, and thus is quite difficult to tackle directly. By applying the polyhedral annexation method and the deep deterministic policy gradient (DDPG) algorithm, we develop an effective algorithm to derive the closed-form solution for the optimal 3D deployment of the UAV, and find the solution for the hybrid beamformer. Two resource allocation algorithms for partial and binary offloading patterns are thereby proposed. Simulation results verify that our designed algorithms achieve a significant computation performance enhancement as compared to the benchmark schemes.

Index Terms—Hybrid beamforming, mobile edge computing, non-orthogonal multiple access, unmanned aerial vehicle, wireless power transfer

I. INTRODUCTION

THE fast proliferation in the Internet-of-Things (IoT) applications has fuelled an exponential growth of IoT devices, including smartphones, wearable devices and wireless sensors, which are widely deployed to support diverse smart applications (e.g., smart cities, automatic manufacturing and smart homes) [1]. However, many of these intelligent applications, such as augmented reality and autonomous navigation, are computationally-intensive and latency-sensitive, which are extremely difficult for IoT devices to handle due to their limited computing capacity. Mobile edge computing (MEC) can potentially serve as an effective technique for enhancing the computing capacity of IoT devices through offloading. With MEC, the IoT devices can offload partial or entire computation missions to the computing servers that are located at the network edge, for instance the base stations (BSs) [2], [3]. In particular, there are two types of working modes in the MEC paradigms, partial and binary offloading. In the partial offloading pattern, the computation missions at IoT devices are

partitioned into two parts, one of which is processed locally at the IoT devices whilst the other part is transmitted for edge execution. In the binary offloading pattern, the entire computation missions are accomplished either at the IoT devices or at the nearby MEC servers [2], [3].

Recently, non-orthogonal multiple access (NOMA) has been viewed as a potential technique for the fifth generation (5G) and beyond 5G (B5G) wireless networks [4], [5]. It has been confirmed that combining MEC and NOMA can reduce the latency and energy cost, and therefore enhance the performance of computation offloading in the MEC paradigms [6]–[8]. In [6], by applying the multi-antenna NOMA technique, weighted sum-energy minimization problems in two working modes were studied in multiuser MEC networks, where the user's central processing unit (CPU) frequencies and transmit power as well as the rate for offloading were jointly optimized. The authors in [7] aimed at minimizing the completion time and energy expenditure of all users in a NOMA-based uplink MEC network. In [8], a framework for computation efficiency had studied in a distributed NOMA-based MEC network, and solved by the Dinkelbach-based iterative algorithm and Karush-Kuhn-Tucker (KKT) conditions, respectively. Nevertheless, when the IoT devices are placed in an area where communication facilities are sparsely distributed, it is not efficient for MEC servers to provide computing services.

Due to the advantages of autonomy, flexibility and mobility, unmanned aerial vehicles (UAVs) can be rapidly deployed for providing reliable services for users in rural and geographically constrained areas [9]. Therefore, the application of UAVs within MEC networks can eliminate the aforementioned shortcomings since they can further shorten the transmission distance and increase the channel gain [10]–[13]. In [10], a total energy minimization problem was studied in a UAV-aided MEC system, where computation resource allocation and UAV trajectory design were considered. A penalty dual decomposition (PDD)-based algorithm was studied in [11] to minimize the maximum task completion time in UAV-aided MEC systems. An alternating optimization scheme for a multiuser aerial MEC system was proposed in [12] to minimize the energy cost, in which the location of the UAV, the time allocation and the task partition were taken into account. Based on the aforementioned research on single UAV solutions, a two-layer optimization scheme for a multi-UAV-aided MEC system was investigated in [13] to reduce

the energy expenditure, where the UAV position and task assignment were optimized.

On the other hand, the wireless power transfer (WPT) has been viewed as a potential technique to prolong the battery-life of IoT devices [14], [15]. Therefore, the integration of MEC and WPT can enhance the computing capacity of IoT devices due to the extension of MEC service time [2], [16]–[18]. In [2], a coordinate descent method and an alternating direction method were exploited to maximize the weighted sum computation rate of the system in a multi-user wireless-powered MEC network. Two alternative schemes were designed in [16] to maximize the weighted sum computation rates of users by considering the CPU frequencies, the offloaded time and the transmission power as well as the UAV's trajectory in a UAV-aided MEC wireless-powered system. This work has been recently extended in [17] to achieve the computation efficiency enhancement in a wireless-powered MEC network, in which energy harvesting time, CPU frequencies, upload time and transmission power were jointly optimized. A successive convex approximation (SCA) method and an iterative algorithm were proposed in [18] to minimize the consumed energy in a UAV-aided wireless-powered MEC system.

In fact, although the computation performance of IoT devices can be improved by WPT, the performance gain is very limited. This is because the harvested energy is significantly degraded by the severe path loss. To tackle this problem, energy beamforming is used to focus the transmitted energy on the receivers for improving the energy transfer efficiency. However, few works have focused on applying the beamforming technique within wireless-powered MEC networks [19]. By applying the maximum ratio transmission (MRC) energy beamforming technique, the authors in [19] investigated the transmission energy consumption minimization framework in a wireless-powered MEC system.

A. Main Contributions

Previous works focus on studying the resource allocation problem for NOMA-aided MEC networks [6]–[8], where the UAVs and WPT are not considered to provide energy supply and computing services for cell-edge users. On the other hand, the works in [10]–[13] aim to minimize the energy expenditure and latency in UAV-aided MEC networks, but do not exploit the NOMA and the WPT for improving the computing capacity of IoT devices. In addition, the works in [2], [16]–[18] focus on investigating the resource management schemes in UAV-aided wireless-powered MEC systems, which cannot simultaneously support multiple users offloading their tasks to computing systems. The work in [19] proposed to apply the energy beamforming within wireless power MEC networks. However, this framework cannot be directly used to more general multi-user environments since only a single user is considered. Motivated by the aforementioned observations, we consider a hybrid beamforming design and resource allocation for sum computation rate maximization in a multiuser UAV-aided wireless-powered MEC network. Our contributions are summarized as follows.

- We formulate the design of hybrid beamforming and resource allocation for IoT devices in a UAV-aided

wireless-powered MEC network under partial and binary offloading patterns. We aim to maximize the sum computation rate at all IoT devices while satisfying the constraint of energy harvesting and coverage. The considered optimization problem is non-convex involving joint optimization of the UAV's 3D placement and the hybrid beamforming matrices as well as computation resource allocation, which is quite difficult to tackle directly. Thus, we first design the 3D placement of the UAV and hybrid beamforming matrices, and then two resource allocation algorithms for the corresponding computation modes are presented.

- For the 3D placement and hybrid beamforming design, we first formulate the energy harvesting maximization problem with the coverage constraint as a convex maximization problem. By applying the polyhedral annexation method, we design the sequential unconstrained convex minimization (SUCM) based placement optimization algorithm to achieve the optimal 3D placement of the UAV. After that, a learning-based two stage hybrid beamforming scheme is proposed to optimize the hybrid beamforming matrices.

- In the case of partial offloading, the sum computation rate maximization problem is expressed as a mixed combinatorial non-convex optimization problem. Inspired by the alternative optimization method and Lagrange dual method, we propose an effective resource allocation scheme to tackle this problem.

- In the case of binary offloading, we develop a resource allocation scheme to handle the decision variables in an iterative manner for a given mode selection decision. Furthermore, by applying the bisection method, we present a channel-gain-based mode selection algorithm to optimize the computing modes.

- Numerical results verify that significant computation performance gain can be achieved through our proposed algorithms as compared to the benchmark schemes, thereby demonstrating the advantages of integrating hybrid beamforming and the NOMA into UAV-aided wireless-powered MEC networks.

B. Organization and Notation

The remainder of this paper is organized as follows. The system model and the sum computation rate maximization problem under the partial and binary offloading are proposed in Section II. In Section III, a SUCM-based placement optimization algorithm and a learning-based two stage hybrid beamforming design are proposed. Two resource allocation algorithms for the partial and binary offloading are discussed in Section IV and Section V, respectively. Numerical results and the conclusion are discussed in Section VI and Section VII.

The following notations are used in this paper. $\mathbf{A}$ is a matrix. $\mathbf{a}^T$ and $\mathbf{a}^H$ denote the transpose and complex conjugate transpose of the vector $\mathbf{a}$. $\|\mathbf{a}\|$ denotes the Euclidean norm. In addition, $\mathbf{R}_+(\mathbf{R}_-)$ represents the set of nonnegative (negative) real numbers.
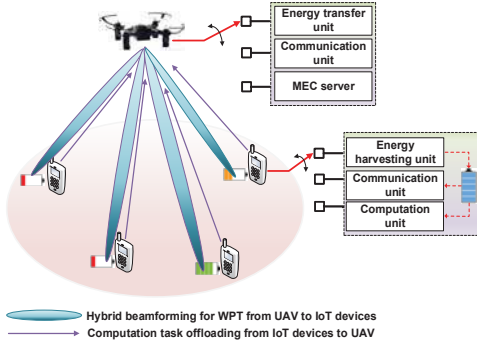
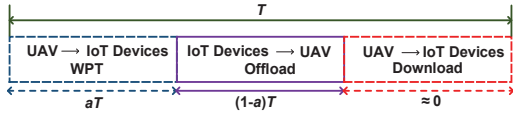**Fig. 1:** Illustration of a multiuser UAV-aided wireless powered MEC system with hybrid beamforming.

Fig. 2: A harvest-then-offload protocol in the UAV-aided wireless powered MEC system.

II. SYSTEM MODEL AND PROBLEM FORMULATION

A. System Model

As depicted in Fig. 1, we consider a UAV-aided wireless powered MEC system with a UAV and K IoT devices, where the UAV is setup with an $M \times N$ rectangular antenna array and all IoT devices have single antenna. In particular, the UAV is mounted with a radio frequency (RF) energy transmitter and a communication unit as well as an MEC server, while each device is mounted with an energy harvesting unit, a communication unit as well as a computation unit [2]. The computation unit of each device is a micro-processor that can only perform simple tasks [2], [16].

It is assumed that all devices need to complete a certain computing task during a given period T. As shown in Fig. 2, a harvest-then-offload protocol is exploited, in which the whole period T contains three phases. In the first phase with duration aT ($a \in [0,1]$), the UAV generates multi-beams to broadcast wireless energy to all IoT devices. Subsequently, IoT devices store the RF energy with the energy harvesting unit, and then transmit the computation tasks to the UAV platform in the second phase with time duration $(1-a)T$. After receiving the offloaded tasks, the UAV executes and replies to the corresponding devices during the third phase. Since the computing capacity of the UAV is much greater than the IoT devices, the data processing and downloading time for the UAV is neglected [2].

In general, the UAV's 2D horizontal location is denoted as $z_u = (x_u, y_u)$, with its altitude as h_u. The location of the device k on the ground is denoted as $z_k = (x_k, y_k)$, where $k \in \mathcal{M} = \{1, 2, \cdots K\}$. The UAV can be flexibly deployed and fly at relatively high altitudes, such that the UAV-ground channels are characterized by line-of-sight (LoS) links. Thus,
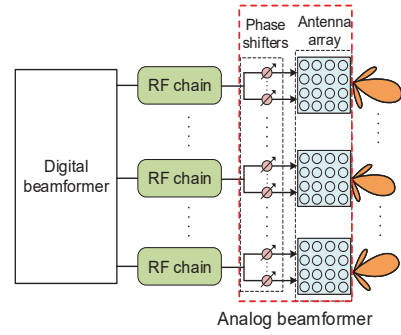

Fig. 3: A hybrid beamforming structure for energy beamforming.

the channel between the UAV and device k is given by [9]

$$\mathbf{h}_k = \sqrt{\beta_0 d_k^{-\alpha}} \mathbf{a}(\theta, \phi), \quad (1)$$

where α ($\alpha \geq 2$) and $d_k = \sqrt{(x_k - x_u)^2 + (y_k - y_u)^2 + h_u^2}$ indicate the path loss exponent and the distance between the UAV and the device k, respectively. Also, β_0 is the channel power gain at the reference distance of $d_0 = 1$ m. Let the wavelength and the spacing between antenna elements be denoted by λ and d_{array}. The steering vector $\mathbf{a}(\theta, \phi)$ of an $M \times N$ antenna array can be further represented by [9]

$$\mathbf{a}(\theta, \phi) = [1, \cdots, e^{j2\pi/\lambda d_{array} \sin(\theta)[(m-1)\cos(\phi)+(n-1)\sin(\phi)]},$$
$$\cdots, e^{j2\pi/\lambda d_{array} \sin(\theta)[(M-1)\cos(\phi)+(N-1)\sin(\phi)]}]^T, \quad (2)$$

where m and n represent the indices of the antenna elements in the xy-plane, respectively, and (θ, ϕ) represents the steering angles.

In practice, the number of RF chains supported at the transmitters is much less than the number of antennas due to hardware constraints [20]. Thus, we consider a hybrid beamforming structure for energy beamforming at the UAV, as shown in Fig. 3, which consists of an analog beamformer and a digital beamformer [21]. The antenna array is partitioned into several sub-arrays, wherein each RF chain is connected to a sub-array and the number of antenna elements per sub-array is N_a^t. It is assumed that the total number of RF chains in the hybrid beamforming architecture is equal to the number of IoT devices, i.e, $N_{RF} = K$. The total number of antenna elements can be calculated by $M \cdot N = N_{RF} \cdot N_a^t$. Then, the channel power gain from the UAV to the device k is expressed as

$$|\mathbf{h}_k^H \mathbf{F} \mathbf{w}_k|^2 = \frac{\beta_0}{[(x_k - x_u)^2 + (y_k - y_u)^2 + h^2]^{\alpha/2}} |\mathbf{B}_k|^2, \quad (3)$$

where $\mathbf{B}_k = \mathbf{a}^H(\theta, \phi)\mathbf{F}\mathbf{w}_k$ and $\mathbf{W} = [\mathbf{w}_1, \mathbf{w}_2, \cdots, \mathbf{w}_K]^T$ denotes the $N_{RF} \times K$ digital beamforming matrix. $\mathbf{F}$ represents the analog beamforming matrix given by

$$\begin{bmatrix} \mathbf{a}(\theta_1, \phi_1) & \mathbf{0}_{N_a^t} & \cdots & \mathbf{0}_{N_a^t} \\ \mathbf{0}_{N_a^t} & \mathbf{a}(\theta_2, \phi_2) & \cdots & \mathbf{0}_{N_a^t} \\ \vdots & \vdots & \ddots & \vdots \\ \mathbf{0}_{N_a^t} & \mathbf{0}_{N_a^t} & \cdots & \mathbf{a}(\theta_{N_{RF}}, \phi_{N_{RF}}) \end{bmatrix}. \quad (4)$$

The diagonal entry $\mathbf{f}_i = \mathbf{a}(\theta_i, \phi_i)$ refers to the analog steering vector for the ith sub-array, $i \in \{1, 2, \cdots, N_{RF}\}$, and (θ_i, ϕ_i)

corresponds to the designed steering angles.

Note that the harvested energy at device k can be shown to be

$$E_k = \tau_0 \xi_0 P_0 |\mathbf{h}_k^H \mathbf{F} \mathbf{w}_k|^2, \tag{5}$$

where P_0 indicates the transmit power of the UAV and τ_0 represents the energy harvesting time. $\xi_0 (0 < \xi_0 < 1)$ denotes the energy conversion efficiency.

B. Partial Offloading

1) Local Computing: Similar to [2], [16], IoT devices can perform local computation and task offloading as well as harvesting energy simultaneously since the energy harvesting unit, communication unit and the computation unit are separated. Let the number of computation cycles required for executing one bit of raw data be denoted by C. We denote the CPU frequency of device k as f_k, which holds $f_k \le f_{max}$. The computation rate of device k is expressed as

$$r_{L,k}^{Par} = \frac{f_k t_k}{CT}, \ k \in \mathcal{M}, \tag{6}$$

where $0 < t_k < T$ is the computation time of the kth device. Accordingly, the consumed energy at device k is given by

$$E_{L,k}^{Par} = \tau_k f_k^3 t_k, \ k \in \mathcal{M}, \tag{7}$$

where τ_k denotes the effective capacitance coefficient.

2) Offloading Computation: Instead of time division multiple access (TDMA), we apply the NOMA scheme that enables all the IoT devices to send tasks to the UAV simultaneously [22], [23]. The channel power gain from the kth device to the UAV is written as [18]

$$g_k = \frac{\beta_0}{[(x_k - x_u)^2 + (y_k - y_u)^2 + h_u^2]^{\alpha/2}}. \tag{8}$$

Without loss of generality, the channel power gains between IoT devices and the UAV are arranged in an ascending order $g_1 < g_2 < \cdots < g_K$. Let B and P_k denote the communication bandwidth and the transmit power of the kth device. The achievable offloading rate from the kth device to the UAV under a given period $(1-a)T$ is then given by

$$r_{o,k}^{Par} = \begin{cases} B(1-a)\log_2 \left(1 + \dfrac{P_k g_k}{\sum_{i=k+1}^{K} P_i g_i + N_0}\right), \\ \qquad\qquad\qquad 1 \le k \le K-1, \\ B(1-a)\log_2 \left(1 + \dfrac{P_k g_k}{N_0}\right), \\ \qquad\qquad\qquad k = K, \end{cases} \tag{9}$$

where N_0 represents the receiver noise power. Thus, from (6) and (9), the total computation rate of device k is expressed as

$$r_{o,k}^{Par} = \begin{cases} \dfrac{f_k t_k}{CT} + B(1-a)\log_2 \left(1 + \dfrac{P_k g_k}{\sum_{i=k+1}^{K} P_i g_i + N_0}\right), \\ \qquad\qquad\qquad 1 \le k \le K-1, \\ \dfrac{f_k t_k}{CT} + B(1-a)\log_2 \left(1 + \dfrac{P_k g_k}{N_0}\right), \\ \qquad\qquad\qquad k = K. \end{cases} \tag{10}$$

Since the energy consumed by the IoT devices during task execution comes from the harvested energy, it needs to satisfy the following energy harvesting constraints

$$\tau_k f_k^3 t_k + P_k(1-a)T \le aT\xi_0 P_0 |\mathbf{h}_k^H \mathbf{F} \mathbf{w}_k|^2, k \in \mathcal{M}, \tag{11}$$

$$aT\xi_0 P_0 |\mathbf{h}_k^H \mathbf{F} \mathbf{w}_k|^2 \le T\xi_0 P_0 |\mathbf{h}_k^H \mathbf{F} \mathbf{w}_k|^2 \le \tau_k f_{max}^3 T, k \in \mathcal{M}. \tag{12}$$

From (12), it can be shown that the harvested energy can be drained when the IoT devices operate at the maximum computing speed [2].

C. Binary Offloading

Let the set of IoT devices operate in local computation and task offloading be denoted by $\mathcal{M}_0 = \{1, \cdots, l_0\}$ and $\mathcal{M}_1 = \{1, \cdots, l_1\}$, where $\mathcal{M} = \mathcal{M}_0 \cup \mathcal{M}_1 = \{1, \cdots, K\}$ and $\mathcal{M} = \mathcal{M}_0 \cap \mathcal{M}_1 = \{\emptyset\}$.

1) Local Computing: For device $k \in \mathcal{M}_0$, all the accumulated energy is exploited for local computation. The computation rate and consumed energy of device k can be expressed as

$$r_{L,k}^{bin} = \frac{f_k t_k}{CT}, \quad \forall k \in \mathcal{M}_0, \tag{13}$$

$$E_{L,k}^{bin} = \tau_k f_k^3 t_k, \quad \forall k \in \mathcal{M}_0. \tag{14}$$

2) Offloading Computation: In this case, each device in $\mathcal{M}_1$ consumes all the accumulated energy to transmit their tasks to the UAV for edge computing. The achievable offloading rate from the kth device to the UAV is written as

$$r_{o,k}^{bin} = \begin{cases} B(1-a)\log_2 \left(1 + \dfrac{P_k g_k}{\sum_{i=k+1}^{K} P_i g_i + N_0}\right), \\ \qquad\qquad \forall k \in \mathcal{M}_1, 1 \le k \le K-1, \\ B(1-a)\log_2 \left(1 + \dfrac{P_k g_k}{N_0}\right), \\ \qquad\qquad \forall k \in \mathcal{M}_1, k = K. \end{cases} \tag{15}$$

Correspondingly, the energy harvesting constraints are given by

$$\tau_k f_k^3 t_k \le aT\xi_0 P_0 |\mathbf{h}_k^H \mathbf{F} \mathbf{w}_k|^2, k \in \mathcal{M}_0, \tag{16}$$

$$P_k(1-a)T \le aT\xi_0 P_0 |\mathbf{h}_k^H \mathbf{F} \mathbf{w}_k|^2, k \in \mathcal{M}_1. \tag{17}$$

D. Problem Formulation

1) Partial Offloading: First, we consider the case of the partial offloading mode, and the sum computation rate maximization problem can be written as

$$\text{(P1)}: \max_{\substack{x_u, y_u, h_u, \mathbf{W}, \mathbf{F}, \\ a, P_k, t_k, f_k}} \sum_{k \in \mathcal{M}} \left[\frac{f_k t_k}{CT} \right.$$

$$\left. + B(1-a)\log_2 \left(1 + \frac{P_k g_k}{\sum_{i=k+1}^{K} P_i g_i + N_0}\right) \right] \tag{18a}$$

$$\text{s.t.} \ \tau_k f_k^3 t_k + P_k(1-a)T \le aT\xi_0 P_0 |\mathbf{h}_k^H \mathbf{F} \mathbf{w}_k|^2, k \in \mathcal{M}, \tag{18b}$$

$$\|z_k - z_u\|^2 \le h_u^2 \tan^2 \Theta, \tag{18c}$$

$$h_{min} \le h_u \le h_{max}, \tag{18d}$$

$$0 \leq t_k \leq T, \tag{18e}$$

$$0 \leq a \leq 1, \tag{18f}$$

$$P_k \geq 0, \tag{18g}$$

$$0 \leq f_k \leq f_{max}. \tag{18h}$$

Constraint (18b) is the energy harvesting constraint for all the IoT devices. Constraint (18c) is the area coverage constraint that the horizontal distance between the IoT devices and the UAV cannot exceed $h_u \tan \Theta$, where 2Θ represents the effective illumination angle [9]. Constraint (18d) denotes the boundary constraint for the UAV's flight altitude. Constraint (18e) ensures that the computation time for IoT devices is no longer than the whole period T. Constraint (18f) is the time constraint for WPT. Constraints (18g) and (18h) correspond to the computation offloading power constraint and the CPU frequency constraint, respectively. Problem (P1) is a mixed combinatorial non-convex optimization problem due to the coupling variables.

2) Binary Offloading: Next, we consider the case in the binary offloading pattern, and the sum computation rate maximization problem can be written as

$$(\text{P2}) : \max_{\substack{x_u,y_u,h_u,\mathbf{W},\mathbf{F}, \\ a,P_k,t_k,f_k,\alpha_k}} \sum_{k \in \mathcal{M}} \left[(1-\alpha_k)\frac{f_k t_k}{CT} \right.$$
$$\left. + \alpha_k B(1-a)\log_2 \left(1 + \frac{P_k g_k}{\sum_{i=k+1}^K P_i g_i + N_0} \right) \right] \tag{19a}$$

$$\text{s.t. } \tau_k f_k^3 t_k \leq aT\xi_0 P_0 |\mathbf{h}_k^H \mathbf{F} \mathbf{w}_k|^2, k \in \mathcal{M}_0, \tag{19b}$$

$$P_k(1-a)T \leq aT\xi_0 P_0 |\mathbf{h}_k^H \mathbf{F} \mathbf{w}_k|^2, k \in \mathcal{M}_1, \tag{19c}$$

$$\|z_k - z_u\|^2 \leq h_u^2 \tan^2 \Theta, \tag{19d}$$

$$h_{min} \leq h_u \leq h_{max}, \tag{19e}$$

$$0 \leq t_k \leq T, \tag{19f}$$

$$0 \leq a \leq 1, \tag{19g}$$

$$P_k \geq 0, \tag{19h}$$

$$0 \leq f_k \leq f_{max}, \tag{19i}$$

$$\alpha_k \in \{0,1\}. \tag{19j}$$

Constraint (19j) indicates the offloading decision of each task. $\alpha_k = 1$ denotes that the task of device k can be executed on the UAV-enabled MEC server while $\alpha_k = 0$ represents the case that the task can be executed locally. Problem (P2) is a mixed integer non-convex optimization problem, which is NP-hard in general [24].

It should be noted that the optimal solutions of (18) and (19) cannot be achieved by simultaneously optimizing all these decision variables. Thus, we focus on optimizing the variables in an alternative manner. It is observed that $|\mathbf{h}_k^H \mathbf{F} \mathbf{w}_k|^2$ can be independently adjusted to maximize the harvested energy at the IoT devices. Motivated by this, we decouple the considered problem into two subproblems, where the solutions are obtained through two steps. In the first step, the 3D placement of the UAV and the hybrid beamforming matrices should be optimized first for maximizing the harvested energy at the IoT devices. Then, based on the harvesting energy constraint, two resource allocation algorithms are properly designed to

maximize the sum computation rate at the IoT devices.

III. 3D PLACEMENT FOR UAV AND HYBRID BEAMFORMING FOR WPT

Since the hybrid beamforming design needs to acquire the beam scanning angles, the UAV's 3D placement should be determined first. Therefore, we first present an effective algorithm to optimize the 3D position of the UAV. Then, we propose a learning-based two-stage hybrid beamforming design to optimize the hybrid beamforming matrices.

A. Optimal UAV 3D Placement

To determine the 3D location of the UAV, we study the following energy harvesting maximization problem:

$$(\text{P3}) : \max_{\substack{x_u,y_u,h_u, \\ \mathbf{W},\mathbf{F}}} \sum_{k=1}^K aT\xi_0 P_0 |\mathbf{h}_k^H \mathbf{F} \mathbf{w}_k|^2 \tag{20a}$$

$$\text{s.t. } \|z_k - z_u\|^2 \leq h_u^2 \tan^2 \Theta, \tag{20b}$$

$$h_{min} \leq h_u \leq h_{max}, \tag{20c}$$

$$\sum_{k=1}^K \| \mathbf{F} \mathbf{w}_k \|^2 \leq P_{th}, \tag{20d}$$

where P_{th} denotes the total transmit power budget. For given $\mathbf{W}$ and $\mathbf{F}$, problem (P3) is non-convex due to the non-convexity of 20(a), Constraints (20b) and (20d). Thus, we first focus on solving for (x_u, y_u) with fixed h_u. With $A_k = aT\xi_0 P_0 \beta_0 |\mathbf{B}_k|^2$, $\zeta_k(x_u, y_u) = (x_k - x_u)^2 + (y_k - y_u)^2 + h_u^2$ and $\eta_k(\zeta_k(x_u, y_u)) = A_k[\zeta_k(x_u, y_u)]^{-\alpha/2}$, problem (P3) is expressed as

$$(\text{P3.1}) : \max_{x_u,y_u} \sum_k \eta_k(\zeta_k(x_u, y_u)). \tag{21}$$

Note that in problem (P3.1), $\zeta_k(x_u, y_u)$ is convex over (x_u, y_u) and $\eta(\cdot)$ is a strictly convex function and strictly decreasing on $\mathbf{R}^+$. Since $\lim_{x_u,y_u \to \infty} \zeta_k(x_u, y_u) = +\infty$ and $\lim_{\zeta_k(x_u, y_u) \to \infty} \eta_k(\zeta_k(x_u, y_u)) = 0$, it can be confirmed that problem (P3.1) is neither a convex nor concave optimization problem [25], [26]. Thus, problem (P3.1) cannot be tackled using convex optimization methods. Therefore, we propose a SUCM-based placement optimization algorithm to deal with problem (P3.1).

To facilitate the application of the SUCM-based placement optimization algorithm, we transform problem (P3.1) into problem (P3.2) by using an auxiliary variable $\mathbf{z} = [z_1, z_2, \cdots, z_K]^T$

$$(\text{P3.2}) : \max_{x_u,y_u,\mathbf{z}} \sum_{k=1}^K \eta_k(z_k) \tag{22a}$$

$$\text{s.t. } \zeta_k(x_u, y_u) \leq z_k, \ k = 1, 2, \cdots, K. \tag{22b}$$

Denote

$$\mathcal{D} = \{\mathbf{z} \in \mathbf{R}_+^k : \zeta_k(x_u, y_u) \leq z_k, \ k = 1, 2, \cdots, K,$$
$$\exists (x_u, y_u) \in \mathbf{R}^2\}. \tag{23}$$

From (23), problem (P3.2) can be equivalently represented as

$$(\text{P3.3}): \max_{\mathbf{z} \in \mathcal{D}} \eta(\mathbf{Z}), \tag{24}$$

where $\eta(\mathbf{z}) = \sum_{k=1}^{K} \eta_k(z_k)$. Since $\eta(\mathbf{z})$ is a convex function and $\mathcal{D}$ denotes a compact convex set, problem (P3.3) is recognized as a convex maximization problem [27].

Denote $\mathcal{C} = \{\mathbf{z} \in \mathbf{R}_+^k : \eta(\mathbf{z}) \leq \eta(\mathbf{z}^*)\}$, $\widetilde{\mathcal{C}} = \{\mathbf{z} - \mathbf{z}_0 \mid \mathbf{z} \in \mathcal{C}\}$ and $\widetilde{\mathcal{D}} = \{\mathbf{z} - \mathbf{z}_0 \mid \mathbf{z} \in \mathcal{D}\}$. Here, $\mathbf{z}_0 = [z_{0,1}, z_{0,2}, \cdots, z_{0,K}]^T$ denotes a feasible point, and $\mathbf{z}^*$ is the best feasible solution. It is observed that the solutions in $\mathcal{C}$ and $\widetilde{\mathcal{C}}$ are not better than $\mathbf{z}^*$. If $\widetilde{\mathcal{D}} \subset \widetilde{\mathcal{C}}$, it follows that $\mathbf{z}^*$ is a global optimal solution; otherwise, it follows that $\mathbf{z}^*$ is a local solution. By introducing the concept of polar set[1], we have the following proposition to determine whether $\widetilde{\mathcal{D}} \subset \widetilde{\mathcal{C}}$.

Proposition 1: Let $\mathcal{V}$ denote the vertex set of the polytope $\mathcal{B}$. $\widetilde{\mathcal{C}}^\text{o} \subset \widetilde{\mathcal{D}}^\text{o}$ satisfies

$$\max_{\mathbf{z} \in \widetilde{\mathcal{D}}} \boldsymbol{v}^T \mathbf{z} \leq 1, \ \forall \boldsymbol{v} \in \mathcal{V}, \tag{25}$$

where $\boldsymbol{v} = [v_1, v_2, \cdots, v_K]^T$. $\widetilde{\mathcal{C}}^\text{o}$ and $\widetilde{\mathcal{D}}^\text{o}$ represent the polar set of $\widetilde{\mathcal{C}}$ and $\widetilde{\mathcal{D}}$, respectively. The polytope $\mathcal{B}$ satisfies $\widetilde{\mathcal{C}}^\text{o} \subset \mathcal{B} \subset \mathbf{R}_-^K$ [26].

Proof: It is noted that by applying the property of the polar set, (25) holds which implies that $\boldsymbol{v} \in \widetilde{\mathcal{D}}^\text{o}, \ \forall \boldsymbol{v} \in \mathcal{V}$. Because $\mathcal{V} \subset \widetilde{\mathcal{D}}^\text{o}$, $\mathcal{V} \subset \mathcal{B}$ and $\mathcal{B} \subset \widetilde{\mathcal{C}}^\text{o}$, it follows that $\mathcal{B} \subset \widetilde{\mathcal{D}}^\text{o}$ and $\widetilde{\mathcal{C}}^\text{o} \subset \widetilde{\mathcal{D}}^\text{o}$. Therefore, this completes the proof of the Proposition 1. ∎

Proposition 1 states that $\widetilde{\mathcal{D}} \subset \widetilde{\mathcal{C}}$ should satisfy (25). We use Proposition 1 and let $-\boldsymbol{v} = \boldsymbol{w} = [w_1, w_2, \cdots, w_K]^T$. Next, consider problem (P3.2) in (22) and notice that $\widetilde{\mathcal{D}} = \{\mathbf{z} - \mathbf{z}_0 \mid \mathbf{z} \in \mathcal{D}\}$, then the optimal 2D location of the UAV (x_u^*, y_u^*) can be achieved by dealing with the equivalent problem derived from (25) as

$$\min_{x_u, y_u} \ \sum_{k=1}^{K} w_k [\zeta_k(x_u, y_u) - z_{0,k}]. \tag{26}$$

By discarding the constant term $-\boldsymbol{w}^T \mathbf{z}_0$, (26) is expressed as

$$\min_{x_u, y_u} \ \sum_{k=1}^{K} w_k \left[(x_k - x_u)^2 + (y_k - y_u)^2 + h_u^2 \right]. \tag{27}$$

Thus, the closed-form expression of (x_u^*, y_u^*) from the above problem is given by

$$x_u^* = \frac{\sum_{k=1}^{K} w_k x_k}{\sum_{k=1}^{K} w_k}, \quad y_u^* = \frac{\sum_{k=1}^{K} w_k y_k}{\sum_{k=1}^{K} w_k}. \tag{28}$$

According to [26], the optimal solution of problem (P3.3) can be obtained by the polyhedral annexation procedure. In particular, we first initiate a polytope $\mathcal{B}^{(1)}$ with the vertex set $\mathcal{V}^{(1)} = \{\boldsymbol{v}^{(1)}\}$ that is constructed by $\mathcal{B}^{(1)} = \left\{ \mathbf{z} \in \mathbf{R}_-^K : -\sum_{k=1}^{K} z_k \leq \frac{1}{\varsigma} \right\}$. The best feasible solution $\mathbf{z}^*$ satisfies $\eta(\mathbf{z}_0) \leq \eta(\mathbf{z}^*)$. Here, ς is small enough such that $\varsigma > 0$ holds, and m is the iteration index. Based on

---

[1] Let the polar set Υ^o for Υ be defined as $\Upsilon^\text{o} = \{\varpi \in \Psi \mid \max_\varpi \varpi^T x \leq 1, x \in \Upsilon, \Psi \subset \mathbf{R}^n\}$ [28]. For some given subsets $\{P, G\}$, if $G^\text{o} \subset P^\text{o}$, it follows that $P \subset G$. Here, G^o and P^o represent the polar set of G and P.

TABLE I: THE SUCM-BASED PLACEMENT OPTIMIZATION ALGORITHM

> 1: Initialize polytope $\mathcal{B}^{(1)}$ with vertex set $\mathcal{V}^{(1)} = \{\boldsymbol{v}^{(1)}\}$;
>   The best-feasible $\mathbf{z}^*$ satisfies $\eta(\mathbf{z}_0) \leq \eta(\mathbf{z}^*)$;
>   Iterate index: m=1;
> 2: **ITERATE**
>   **FOR ALL** $-\boldsymbol{w} \in \mathcal{V}^{(m)}$
>   Calculate $-\psi(\boldsymbol{w})$ and (x_u^*, y_u^*) by solving (27)
>   **END**
> 3: **IF** $\max_{-\boldsymbol{w} \in \mathcal{V}^{(m)}} -\psi(\boldsymbol{w}) + \boldsymbol{w}^T \mathbf{z}_0 \leq 1$
>   **RETURN**;
>   **END**
> 4: Calculate $\overline{\boldsymbol{w}}$ and $\overline{\mathbf{z}}$ using
> $\overline{\boldsymbol{w}} \in \max_{-\boldsymbol{w} \in \mathcal{V}^{(m)}} -\psi(\boldsymbol{w}) + \boldsymbol{w}^T \mathbf{z}_0$ and
> $\overline{z}_k = \zeta_k(\overline{x}_u, \overline{y}_u)$;
> 5: **IF** $\eta(\overline{\mathbf{z}}) > \eta(\mathbf{z}^*)$
>   Update $\mathbf{z}^* = \overline{\mathbf{z}}$;
>   **ELSE**
>   Calculate ε and $\mathcal{B}^{(m+1)}$;
>   **END**
> $m := m + 1$;
> 6: **UNTIL: CONVERGENCE**.

the vertex set $\mathcal{V}^{(m)}$, we calculate $-\psi(\boldsymbol{w})$ and (x_u^*, y_u^*) by solving the problem in (27), where $\psi(\boldsymbol{w})$ is the objection function value of (27). Here, if the optimal value of $\boldsymbol{w}$ satisfies $\max_{-\boldsymbol{w} \in \mathcal{V}^{(m)}} -\psi(\boldsymbol{w}) + \boldsymbol{w}^T \mathbf{z}_0 \leq 1$, it follows that $\mathbf{z}^*$ is a globally optimal solution; otherwise, it follows that $\mathbf{z}^*$ is not a globally optimal solution. Then, we separate the local solutions by the analytic center cutting plane method (ACCPM) [29]. Specifically, we compute $\overline{\boldsymbol{w}}$ and $\overline{\mathbf{z}}$ by $\overline{\boldsymbol{w}} \in \max_{-\boldsymbol{w} \in \mathcal{V}^{(m)}} -\psi(\boldsymbol{w}) + \boldsymbol{w}^T \mathbf{z}_0$ and $\overline{z}_k = \zeta_k(\overline{x}_u, \overline{y}_u)$, respectively. Here, $\overline{x}_u = \frac{\sum_{k=1}^{K} \overline{w}_k x_k}{\sum_{k=1}^{K} \overline{w}_k}$ and $\overline{y}_u = \frac{\sum_{k=1}^{K} \overline{w}_k y_k}{\sum_{k=1}^{K} \overline{w}_k}$. If $\eta(\overline{\mathbf{z}}) > \eta(\mathbf{z}^*)$, we update $\mathbf{z}^*$ by $\overline{\mathbf{z}}$. On the other hand, if $\eta(\overline{\mathbf{z}}) \leq \eta(\mathbf{z}^*)$, we determine the cutting planes ε and update the polytope $\mathcal{B}^{(m+1)}$ by computing $\varepsilon = \sup\{\rho : \eta(\mathbf{z}_0 + \rho(\overline{\mathbf{z}} - \mathbf{z}_0)) \leq \eta(\mathbf{z}^*)\}$ and $\mathcal{B}^{(m+1)} = \mathcal{B}^{(m)} \cap \{\mathbf{z} : \mathbf{z}^T(\overline{\mathbf{z}} - \mathbf{z}_0) \leq \frac{1}{\varepsilon}\}$. Similarly, we repeat the above procedure to construct a sequential nested polytope for which $\mathcal{B}^{(1)} \supset \mathcal{B}^{(2)} \supset \cdots \supset \mathcal{B}^{(m)} \supset \widetilde{\mathcal{C}}^\text{o}$. The proposed SUCM-based placement optimization algorithm is summarized in TABLE I.

With (x_u^*, y_u^*) as given in TABLE I, it can be verified that (20a) is monotonic decreasing in h_u. From (20b), it follows that the optimal flight altitude h_u^* is given by

$$h_u^* = \max \left\{ \frac{\sqrt{Q_{\max}}}{\tan \Theta}, h_{min} \right\}, \tag{29}$$

where $Q_{\max} = \max_{k=1,\cdots,K} \| z_k - z_u \|^2$. Next, we focus on solving the analog beamformer $\{\mathbf{F}\}$ and the digital beamformer $\{\mathbf{W}\}$ with fixed (x_u^*, y_u^*, h_u^*).

B. MOEA/D Based Analog Beamformer Design

The analog beamformer is designed by beam pattern synthesis. The key idea of beam pattern synthesis is to optimize the sidelobe level (SLL), array gain and beamwidth through

controlling the phases [9]. Mathematically, this can be tackled by a multiobjective optimization framework

$$\min \ F(\boldsymbol{\vartheta}) = (f_1(\boldsymbol{\vartheta}), f_2(\boldsymbol{\vartheta}), f_3(\boldsymbol{\vartheta}))^T$$
$$\text{s.t. } \boldsymbol{\vartheta} \in \mathbf{R}^{M \times N}, \tag{30}$$

where $f_1(\boldsymbol{\vartheta}) = SLL(\boldsymbol{\vartheta})$, $f_2(\boldsymbol{\vartheta}) = \frac{1}{|\mathbf{E}(\theta,\phi)|}$, and $f_3(\boldsymbol{\vartheta}) = \frac{1}{|\Theta_{h,e}|}$. $\boldsymbol{\vartheta} = [\vartheta_{1n}, \cdots, \vartheta_{mn}, \cdots, \vartheta_{MN}]^T$ denotes the phases of the $M \times N$ antenna array. $SLL(\boldsymbol{\vartheta}) = 20 \log \frac{|\mathrm{AF}_{msl}|}{|\mathrm{AF}_{max}|}$ denotes the SLL of the $M \times N$ antenna array [30], where AF_{msl} and AF_{max} represent the array factor of the maximum SLL and the main-lobe, respectively [9]. Note that the array factor of the $M \times N$ antenna array is $\mathrm{AF} = \sum_{m=1}^{M} \sum_{n=1}^{N} I_{mn} \times e^{j2\pi/\lambda d_{array} \sin(\theta)[(m-1)\cos(\phi)+(n-1)\sin(\phi)]+j\vartheta_{mn}}$ [30]. $\mathbf{E}(\theta,\phi) = \mathbf{a}^H(\theta,\phi)\mathbf{F}$ is the synthesized pattern, and $\mathbf{F} = e^{j\boldsymbol{\vartheta}}$. $\Theta_{h,e}$ represents the elevation plane half-power beamwidth. To solve problem (30), a multiobjective evolutionary algorithm (MOEA/D) solution is proposed here. The steps of this algorithm are presented as follows.

- *Input*: Let $\{N_{sub}, \boldsymbol{\beta}^i, S_{nei}, iter\}$ be a set of input parameters. Here, N_{sub} denotes the number of subproblems. $\boldsymbol{\beta}^i = (\beta_1^i, \cdots, \beta_d^i)^T, i = 1, \cdots, N_{sub}, 1 \leq d \leq 3$ is the weight vector of the ith subproblem. S_{nei} represents the number of weight vectors considered to be neighbors of each weight vector and $iter$ is the iteration index.
- *Output*: The output is a non-dominated set ND^2.
- *Initialization*: We first select S_{nei} as the closest weight vectors of $\boldsymbol{\beta}^i$ by calculating the Euclidean distance, whose indices are stored in $\mathcal{C}(i)$. Then, we generate the initial solutions $\boldsymbol{\vartheta}_1, \cdots, \boldsymbol{\vartheta}_{N_{sub}}$ randomly, and then update the F-values $FV_i = F(\boldsymbol{\vartheta}_i)$ and the best-so-far solutions $\mathcal{L} = (L_1, \cdots, L_j, \cdots, L_d)^T$. Here, $L_j = \min\{f_j(\boldsymbol{\vartheta}), \boldsymbol{\vartheta} \in \mathbf{R}^{M \times N}\}$.
- *Update*: For each $i = 1, \cdots, N_{sub}$, we choose two weight vectors $\boldsymbol{\vartheta}_k$ and $\boldsymbol{\vartheta}_l$ from $\mathcal{C}(i)$ and then generate a new solution $\boldsymbol{x}$ by applying the differential evolution (DE) algorithm [32]. Then, we update the best-so-far solutions and the F-value of $\boldsymbol{\vartheta}_i$. Specifically, for $j = 1, \cdots, d$, if $L_j > f_j(\boldsymbol{x})$, it follows that $L_j = f_j(\boldsymbol{x})$; if $g^{te}(\boldsymbol{x} \mid \boldsymbol{\beta}^j, \mathcal{L}) \leq g^{te}(\boldsymbol{\vartheta}_j \mid \boldsymbol{\beta}^j, \mathcal{L})$, it follows that $\boldsymbol{\vartheta}_j = \boldsymbol{x}$ and $FV_j = F(\boldsymbol{x})$. Here, $g^{te}(\boldsymbol{x} \mid \boldsymbol{\beta}^j, \mathcal{L}) = \max_{1 \leq t \leq d}\{\beta_t^j |f_t(\boldsymbol{x}) - L_t|\}$ [31]. $F(\boldsymbol{x})$ will be stored in ND if it dominates other weight vectors, and all weight vectors from ND dominated by $F(\boldsymbol{x})$ are eliminated.
- *Stopping*: The algorithm terminates if the iterations have converged; otherwise, go back to *Update*.

The Pareto solutions can be obtained by the MOEA/D based algorithm, whose convergence performance is similar to [31] and thus we omit it here.

C. DDPG Based Digital Beamformer Design

Based on the optimal 3D placement of the UAV and the analog beamformer, it can be verified that constraint (20b) and

---

^{2}Let $\omega, \nu \in \mathbf{R}^n$, ν is dominated by ω if and only if $\omega_i \leq \nu_i, i \in \{1, \cdots, n\}$ and $\omega_j < \nu_j, \exists j \in \{1, \cdots, n\}$ [31].

(20c) are satisfied, and problem (P3) is then rewritten as

$$(\text{P3.3}) : \max_{\mathbf{W}} \ \sum_{k=1}^{K} aT\xi_0 P_0 |\mathbf{h}_k^H \mathbf{F} \mathbf{w}_k|^2 \tag{31a}$$

$$\text{s.t. } \sum_{k=1}^{K} \| \mathbf{F}\mathbf{w}_k \|^2 \leq P_{th}, \tag{31b}$$

Problem (P3.3) can be efficiently solved using the semi-definite relaxation (SDR) approach. By introducing $\overline{\mathbf{h}}_k = \mathbf{h}_k^H \mathbf{F}$, $\mathbf{H} = \sum_{k=1}^{K} aT\xi_0 P_0 \overline{\mathbf{h}}_k \overline{\mathbf{h}}_k^H$, $\mathbf{S} = \mathbf{F}\mathbf{F}^H$, $\overline{\mathbf{W}}_k = \mathbf{w}_k \mathbf{w}_k^H$, problem (P3.3) can be relaxed as

$$(\text{P3.4}) : \max_{\overline{\mathbf{W}}_k} \ \sum_{k=1}^{K} \text{tr}(\mathbf{H}\overline{\mathbf{W}}_k) \tag{32a}$$

$$\text{s.t. } \sum_{k=1}^{K} \text{tr}(\mathbf{S}\overline{\mathbf{W}}_k) \leq P_{th}, \tag{32b}$$

$$\overline{\mathbf{W}}_k \succeq 0. \tag{32c}$$

Problem (P3.4) is a convex semi-definite programming (SDP) problem, and hence can be tackled by the interior-point methods [25]. However, the interior-point methods have high memory requirements and thus are difficult to implement in large-scale problems, i.e., matrices with large size. Consequently, we propose a learning-based method to optimize the digital beamformer. In this paper, we adopt the deep deterministic policy gradient (DDPG) instead of the deep Q network (DQN) which is due to the fact that DDPG is the only algorithm which can handle continuous value action space and provide a continuous decision value.

For the considered UAV-aided wireless-powered MEC system, we have obtained the analog beamforming matrix by the MOEA/D based algorithm, which will act as the basis of our digital precoding matrix design. The DDPG algorithm has three elements, i.e., states, actions and rewards, and the DDPG process can be described as follows

- *Initialization:* Initialize the critic network $Q(s, a|\theta^Q)$ with weights θ^Q and actor network $\mu(s|\theta^\mu)$ with θ^μ. Initialize the target network Q' with weights $\theta^{Q'}$ and target network μ' with $\theta^{\mu'}$, while $\theta^{Q'} = \theta^Q$ and $\theta^{\mu'} = \theta^\mu$. Initialize the replay memory R.
- *Loop:*

1) Observe the status s_t. The status consists of the distance between the UAV and the IoT devices as well as the unwrapped analog precoding matrix, i.e., $[d_k, real(\mathbf{f}_1), imag(\mathbf{f}_1), \ldots, real(\mathbf{f}_{N_a^t}), imag(\mathbf{f}_{N_a^t})]$.
2) Generate an action as $a_t = \mu(s_t|\theta^\mu) + \mathcal{N}_t$, where $\mathcal{N}_t$ is an exploration process and t is the iteration index. $\mu(s_t|\theta^\mu)$ is an action generation policy. This exploration process guarantees that the action choice will not fall into a local optimum.
3) Execute action a_t and calculate the reward r_t, while observing the next time slot status s_{t+1}. Then, put the memory (s_t, a_t, r_t, s_{t+1}) into the replay memory R.
4) Randomly select a training batch of N from R, that

is (s_i, a_i, r_i, s_{i+1}), $i \in \{1, \cdots, N\}$. Set $y_i = r_i + \gamma Q'(s_{i+1}, \mu'(s_{i+1}|\theta^{\mu'})|\theta^{Q'})$ and calculate the result.

5) Update the critic network and the actor policy by minimizing the loss $L = \frac{1}{N} \sum_i (y_i - Q(s_i, a_i|\theta^Q))^2$ and the gradient $\Delta_{\theta^\mu} \mathcal{J} \approx \frac{1}{N} \sum_i \Delta_a Q(s, a|\theta^Q)|_{s=s_i, a=\mu(s_i)} \Delta_{\theta|mu} \mu(s|\theta^\mu)|_{s_i}$, respectively. Update the target network weights as $\theta^{Q'} \leftarrow \tau\theta^Q + (1-\tau)\theta^{Q'}$ and $\theta^{\mu'} \leftarrow \tau\theta^\mu + (1-\tau)\theta^{\mu'}$.

- *Stopping:* The algorithm terminates if the loop process reaches a predetermined number.
- *Output:* The digital precoding matrix.

IV. NOMA-BASED RESOURCE ALLOCATION ALGORITHM IN PARTIAL OFFLOADING MODE

In this section, a NOMA-based resource allocation algorithm in partial offloading mode is proposed, where the WPT time allocation a, the transmit power of IoT devices P_k, the computation time of IoT devices t_k and the CPU frequencies f_k are jointly optimized in an iterative manner.

With solved (x_u^*, y_u^*, h_u^*), $\mathbf{F}^*$ and $\mathbf{W}^*$, problem (P1) is expressed as

$$(P4): \max_{a, P_k, t_k, f_k} \sum_{k=1}^{K} \left[\frac{f_k t_k}{CT} \right.$$
$$\left. + B(1-a)\log_2\left(1 + \frac{P_k g_k}{\sum_{i=k+1}^{K} P_i g_i + N_0}\right) \right] \quad (33a)$$
$$\text{s.t. } \tau_k f_k^3 t_k + P_k(1-a)T \le aT\xi_0 P_0 |\mathbf{h}_k^H \mathbf{F} \mathbf{w}_k|^2, k \in \mathcal{M}, \quad (33b)$$
$$0 \le t_k \le T, \quad (33c)$$
$$0 \le a \le 1, \quad (33d)$$
$$P_k \ge 0, \quad (33e)$$
$$0 \le f_k \le f_{max}. \quad (33f)$$

Problem (P4) is non-convex. To tackle this problem, the considered problem is decoupled into two subproblems. Particularly, for given a and t_k, problem (P4) is written as

$$(P4.1): \max_{P_k, f_k} \sum_{k=1}^{K} \left[\frac{f_k t_k}{CT} \right.$$
$$\left. + B(1-a)\log_2\left(1 + \frac{P_k g_k}{\sum_{i=k+1}^{K} P_i g_i + N_0}\right) \right] \quad (34a)$$
$$\text{s.t. } \tau_k f_k^3 t_k + P_k(1-a)T \le aT\xi_0 P_0 |\mathbf{h}_k^H \mathbf{F} \mathbf{w}_k|^2, k \in \mathcal{M}, \quad (34b)$$
$$P_k \ge 0, \quad (34c)$$
$$0 \le f_k \le f_{max}. \quad (34d)$$

Problem (4.1) is still a non-convex problem due to the second term of (34a). By applying the logarithmic transformation, we transform $\sum_{k=1}^{K} B(1-a)\log_2\left(1 + \frac{P_k g_k}{\sum_{i=k+1}^{K} P_i g_i + N_0}\right)$ as

$$B(1-a)\log_2\left(\frac{\sum_{i=1}^{K} P_i g_i + N_0}{N_0}\right). \quad (35)$$

TABLE II: THE RESOURCE ALLOCATION ALGORITHM FOR PARTIAL OFFLOADING MODE

1: Initialize $(\lambda_k(n), f_k(n), P_k(n), a(n), P_k(n))$;
   Iterate index: n=1;
2: **ITERATE**
   ▷ For given $a^*(n), t_k^*(n)$, obtain $\lambda_k(n)$ by (44), then calculate $f_k^*(n)$ and $P_k^*(n)$ by (37) and (38);
   ▷ For given $f_k^*(n), P_k^*(n)$, solve (P4.3) by CVX, then calculate $a^*(n)$ and $t_k^*(n)$;
   ▷ Set $n \leftarrow n + 1$;
3: **UNTIL: CONVERGENCE;**
4: **OUTPUT:**
   $f_k^* = f_k^*(n), P_k^* = P_k^*(n), a^* = a^*(n), t_k^* = t_k^*(n)$.

Using (35), (P4.1) is expressed as the following equivalent problem

$$(P4.2): \max_{P_k, f_k} \sum_{k=1}^{K} \frac{f_k t_k}{CT}$$
$$+ B(1-a)\log_2\left(\frac{\sum_{i=1}^{K} P_i g_i + N_0}{N_0}\right) \quad (36a)$$
$$\text{s.t. } \tau_k f_k^3 t_k + P_k(1-a)T \le aT\xi_0 P_0 |\mathbf{h}_k^H \mathbf{F} \mathbf{w}_k|^2, k \in \mathcal{M}, \quad (36b)$$
$$P_k \ge 0, \quad (36c)$$
$$0 \le f_k \le f_{max}. \quad (36d)$$

For the objective function given by (36a), $\frac{f_k t_k}{CT}$ is a linear function of the CPU frequency f_k and $B(1-a)\log_2\left(\frac{\sum_{i=1}^{K} P_i g_i + N_0}{N_0}\right)$ is concave with respect to P_i. For the constraint $\tau_k f_k^3 t_k + P_k(1-a)T \le aT\xi_0 P_0 |\mathbf{h}_k^H \mathbf{F} \mathbf{w}_k|^2$, the right side $aT\xi_0 P_0 |\mathbf{h}_k^H \mathbf{F} \mathbf{w}_k|^2$ is a constant and the left side $\tau_k f_k^3 t_k + P_k(1-a)T$ is a convex function with respect to f_k and a linear function in regard to P_k. Moreover, the constraints (36c) and (36d) are linear inequality constraints. Thus, problem (P4.2) is a convex optimization problem and can be tackled using convex optimization methods [33]. Next, the Lagrange duality method is applied to achieve the closed-form solutions of the CPU frequencies and the UAV's transmit power for offloading.

Proposition 2: For given WPT time allocation a and computation time t_k, the optimal solution of problem (P4.2) can be given by

$$f_k^* = \sqrt{\frac{1}{3\lambda_k \tau_k CT}}, \quad (37)$$
$$\sum_{m=k}^{K} P_m^* g_m = \left[\frac{Bg_k}{\lambda_k T \ln 2} - N_0\right]^+, \quad (38)$$

where $[x]^+$ denotes $\max(x, 0)$.

Proof: Please refer to Appendix A for the proof of Proposition 2. ∎

To obtain the optimal solution of problem (P4.2), we adopt the subgradient approach where the dual variables are updated through iteration process [34]. Therefore, in the $(n + 1)$th

iteration, the dual variable $\lambda_k(n+1)$ is given by

$$\lambda_k(n+1) = [\lambda_k(n) - \delta\Delta\lambda_k(n)]^+, \quad (44)$$

where δ represents a sufficiently small positive step-size. $\Delta\lambda_k(n)$ is the corresponding subgradient that is expressed as

$$\Delta\lambda_k(n) = aT\xi_0 P_0|\mathbf{h}_k^H\mathbf{F}\mathbf{w}_k|^2 - \tau_k f_k^3 t_k - P_k(1-a)T. \quad (45)$$

For a given CPU frequency f_k^* and transmit power for offloading P_k^*, problem (P4) is rewritten as

$$(\text{P4.3}) : \max_{a,t_k} \sum_{k=1}^{K}\left[\frac{f_k t_k}{CT}\right.$$
$$\left. + B(1-a)\log_2\left(1 + \frac{P_k g_k}{\sum_{i=k+1}^{K}P_i g_i + N_0}\right)\right] \quad (46a)$$

$$\text{s.t. } \tau_k f_k^3 t_k + P_k(1-a)T \le aT\xi_0 P_0|\mathbf{h}_k^H\mathbf{F}\mathbf{w}_k|^2, k \in \mathcal{M}, \quad (46b)$$

$$0 \le t_k \le T, \quad (46c)$$

$$0 \le a \le 1. \quad (46d)$$

Since the objective function and constraints are linear functions with respect to a and t_k, problem (P4.3) is a linear programming problem. Thus, problem (P4.3) can be tackled effectively through the CVX toolbox [35].

The resource allocation algorithm for tackling problem (P4) is summarized in TABLE II. In each iteration, (36a) is maximized over (f_k, P_k), while keeping (a, t_k)'s fixed. For a given (f_k, P_k), the set of (a, t_k) is obtained via solving problem (P4.3). The algorithm terminates if it converges to a fixed point.

V. NOMA-BASED RESOURCE ALLOCATION ALGORITHM IN BINARY OFFLOADING MODE

In this section, a resource allocation algorithm in binary offloading pattern is studied under given mode selection. Then, a channel-gain-based mode selection method is proposed to optimize the model selection.

A. Resource Allocation Under Given Mode Selection

For given α_k, (x_u^*, y_u^*, h_u^*), $\mathbf{F}^*$ and $\mathbf{W}^*$, problem (P2) is formulated as

$$(\text{P5}) : \max_{a,P_j,t_k,f_k} \sum_{k\in\mathcal{M}_0}\frac{f_k t_k}{CT}$$
$$+ \sum_{j\in\mathcal{M}_1}B(1-a)\log_2\left(1 + \frac{P_j g_j}{\sum_{i=j+1}^{K}P_i g_i + N_0}\right) \quad (47a)$$

$$\text{s.t. } \tau_k f_k^3 t_k \le aT\xi_0 P_0|\mathbf{h}_k^H\mathbf{F}\mathbf{w}_k|^2, k \in \mathcal{M}_0, \quad (47b)$$

$$P_j(1-a)T \le aT\xi_0 P_0|\mathbf{h}_j^H\mathbf{F}\mathbf{w}_j|^2, j \in \mathcal{M}_1, \quad (47c)$$

$$0 \le t_k \le T, k \in \mathcal{M}_0, \quad (47d)$$

$$0 \le a \le 1, \quad (47e)$$

$$P_j \ge 0, j \in \mathcal{M}_1, \quad (47f)$$

$$0 \le f_k \le f_{max}, k \in \mathcal{M}_0. \quad (47g)$$

TABLE III: THE CHANNEL-GAIN-BASED MODE SELECTION ALGORITHM

1: Initialize $g_k, \forall k \in \mathcal{M}$, $\mathbf{D}_{sort} \leftarrow sort(g_k)$, $m = 0$;
2: **REPEAT:**
IF $m = 0$
$\mathcal{M}_1 \leftarrow \{\emptyset\}$;
ELSE
$\mathcal{M}_1 \leftarrow \{1, \cdots, m\}$;
END
Obtain optimal a_m^* and R_{sum}^m using
the Bisection method under $\mathcal{M}_1$ and $\mathbf{D}_{sort}$;
Set $m \leftarrow m + 1$;
3: **UNTIL:** $m = K$;
4: **OUTPUT:**
$R_{sum}^{max} \leftarrow \max(R_{sum}^m)$, $\mathcal{M}_1$.

Similar to (18), problem (P5) is a mixed combinatorial non-convex problem. Note that when the WPT time a is fixed, the CPU frequency f_k and the computation time t_k of each device k ($k \in \mathcal{M}_0$) can be optimized independently without affecting the computation performance of other IoT devices. Moreover, the maximum local computation rate can be obtained by optimizing f_k and t_k. Motivated by this, we then have the following proposition.

Proposition 3: The optimal CPU frequencies and the computation time to maximize the local computation rate subject to the energy harvesting constraint are given by

$$t_k^* = T, \ f_k^* = \left(\frac{a\xi_0 P_0|\mathbf{h}_k^H\mathbf{F}\mathbf{w}_k|^2}{\tau_k}\right)^{\frac{1}{3}}, \forall k \in \mathcal{M}_0. \quad (48)$$

Proof: Please refer to Appendix B for the proof of Proposition 3. ∎

With t_k^* and f_k^* given in (48) and by substituting (35) into problem (P5), problem (P5) is equivalently expressed as

$$(\text{P5.1}) : \max_{a,P_j} \sum_{k\in\mathcal{M}_0} a^{\frac{1}{3}}\left(\frac{\xi_0 P_0|\mathbf{h}_k^H\mathbf{F}\mathbf{w}_k|^2}{\tau_k}\right)^{\frac{1}{3}}\frac{1}{C}$$
$$+ B(1-a)\log_2\left(1 + \frac{\sum_{i=1}^{l_1}P_i g_i}{N_0}\right) \quad (49a)$$

$$\text{s.t. } P_j(1-a)T \le aT\xi_0 P_0|\mathbf{h}_j^H\mathbf{F}\mathbf{w}_j|^2, j \in \mathcal{M}_1, \quad (49b)$$

$$0 \le a \le 1, \quad (49c)$$

$$P_j \ge 0, j \in \mathcal{M}_1. \quad (49d)$$

It can be observed from problem (P5.1) that as the transmission power of the IoT devices P_j increases, so does the sum computation rate. Therefore, the optimal transmission power P_j should be as large as possible within the range of its energy harvesting $aT\xi_0 P_0|\mathbf{h}_j^H\mathbf{F}\mathbf{w}_j|^2$, which can be achieved based on (49b) and is given by

$$P_j^* = \frac{a\xi_0 P_0|\mathbf{h}_j^H\mathbf{F}\mathbf{w}_j|^2}{1-a}, j \in \mathcal{M}_1. \quad (50)$$

From (50), it is observed that the transmission power of the IoT devices depends on the WPT time allocation a. Using (50), the optimal WPT time a^* can be achieved by considering

the following equivalent problem (P5.2) derived from problem (P5.1):

$$(P5.2): \max_a \sum_{k \in \mathcal{M}_0} a^{\frac{1}{3}} \left(\frac{\xi_0 P_0 |\mathbf{h}_k^H \mathbf{F} \mathbf{w}_k|^2}{\tau_k} \right)^{\frac{1}{3}} \frac{1}{C}$$

$$+ B(1-a) \log_2 \left(1 + \frac{\gamma a}{1-a} \right) \tag{51a}$$

$$\text{s.t. } 0 \leq a \leq 1, \tag{51b}$$

where $\gamma = \sum_{i=1}^{l_1} \frac{\xi_0 P_0 |\mathbf{h}_i^H \mathbf{F} \mathbf{w}_i|^2 g_i}{N_0}$. From (51a), the left side $\sum_{k \in \mathcal{M}_0} a^{\frac{1}{3}} \left(\frac{\xi_0 P_0 |\mathbf{h}_k^H \mathbf{F} \mathbf{w}_k|^2}{\tau_k} \right)^{\frac{1}{3}} \frac{1}{C}$ is a concave function with respect to a. The right side $B(1-a) \log_2 \left(1 + \frac{\gamma a}{1-a} \right)$ is also a concave function with respect to a. Thus, problem (P5.2) is a convex optimization problem. Denote $q(a)$ as the first-order derivative of a, which is defined as

$$q(a) = \frac{1}{3} a^{-\frac{2}{3}} \sum_{k \in \mathcal{M}_0} \left(\frac{\xi_0 P_0 |\mathbf{h}_k^H \mathbf{F} \mathbf{w}_k|^2}{\tau_k} \right)^{\frac{1}{3}} \frac{1}{C}$$

$$+ B \left(\frac{(1-a)(\gamma-1)}{\ln 2[(\gamma-1)a+1]} - \log_2 \left(\frac{(\gamma-1)a+1}{1-a} \right) + \frac{1}{\ln 2} \right). \tag{52}$$

Given the concavity of the above problem (P5.2), the optimal WPT time a^* can be achieved at $q(a^*) = 0$. To facilitate the solution, the bisection method is applied to find a^*. Note that when the optimal WPT time allocation a^* in problem (P5.2) is obtained, the corresponding transmission power P_j^* is then achieved.

B. Channel-Gain-Based Mode Selection Optimization

In this subsection, we study the offloading decision of task execution between local execution and task offloading. Since it is hard to jointly optimize K binary variables α_k, an effective algorithm is proposed here. From (35), the achievable transmission rate of IoT devices is independent of the decoding order [36]. Thus, the sum computation rate of all IoT devices is not affected by the NOMA decoding when the set of IoT devices operated in task offloading $\mathcal{M}_1$ and the WPT time allocation a are given. Motivated by this, we propose the channel-gain-based mode selection scheme to determine $\mathcal{M}_1$ by considering the channel characteristics of the UAV-ground links. First, based on the channel power gain $g_k, \forall k \in \mathcal{M}$, all IoT devices are ranked in a descending order. Subsequently, the objective value R_{sum} of problem (P5.2) and the WPT time allocation a are obtained by considering $\mathcal{M}_1 = \{\emptyset\}$ and $\mathcal{M}_1 = \{1, \cdots, m\}, m = 1, \cdots, K$. Finally, the computing mode with the maximum objective value is chosen. The algorithm is outlined in TABLE III.

Remark 1: The complexity of ordering the IoT devices is $\mathcal{O}(K \log_2(K))$. Furthermore, the complexity of the bisection approach with precision parameter σ_0 is $\mathcal{O}(\log_2(1/\sigma_0))$. To sum up, the complexity of the channel-gain-based mode selection algorithm is then $\mathcal{O}(K \log_2(K/\sigma_0))$.

TABLE IV: PARAMETERS SETTINGS

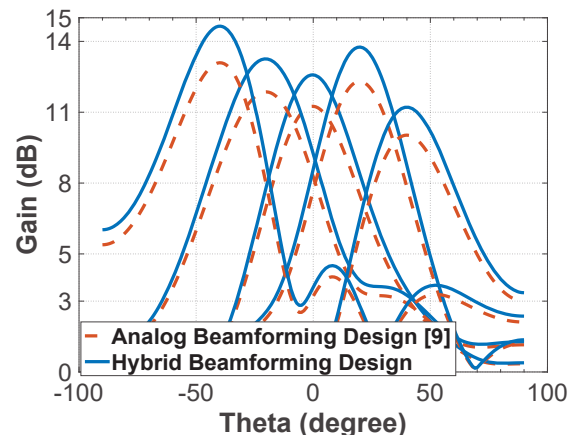| Parameters	Notation	Values
The channel power gain	β_0	-20 dB
The path loss factor	α	2
The energy conversion efficiency	ξ_0	0.8
The transmit power of UAV	P_0	3 W
The communication bandwidth	B	20 MHz
The noise power	N_0	10^{-9} W
The number of cycles for one bit	C	200 cycles/bit
The capacitance coefficient	τ_k	10^{-26}
The whole period	T	1 s
The minimum altitude of UAV	h_{min}	5 m
The maximum altitude of UAV	h_{max}	21 m
The effective illumination angle	2Θ	$80°$

Fig. 4: An example of the beam pattern response for the hybrid beamforming design with $\phi = 90°$.

VI. SIMULATION RESULTS

We provide numerical results to validate the performance of all presented algorithms. For convenience, we assume that the UAV-carried wireless-powered MEC network has $K = 4$ IoT devices, whose positions are $(10, 10)$, $(0, 10)$, $(10, 0)$ and $(0, 0)$, respectively. It is assumed that the 8×8 UAV-mounted antenna array is separated into four 4×4 rectangular arrays. The parameter settings for the resource allocation schemes are similar in [2], [9], [16], and the details of parameter settings are presented in TABLE IV. It should be noted that these parameters settings are selected to illustrate the performance in an example and can be changed to any other values relying on the specific scenario under consideration.

First, we compare the beam pattern response of our designed hybrid beamforming with that of the analog beamforming recently designed in [9]. It is assumed that the excitation amplitude and element spacing of the antenna array are 1 A and 5.5 mm. The beam directions are $(-40°, 90°)$, $(-20°, 90°)$, $(0°, 0°)$, $(20°, 90°)$ and $(40°, 90°)$. It is observed in Fig. 4 that the main lobe responses achieved by our proposed hybrid beamforming outperforms the analog beamforming. This is due to the fact that when the analog beamforming is determined, the digital beamforming weights can be optimized to further improve the gain. Furthermore, the main-lobe gain of
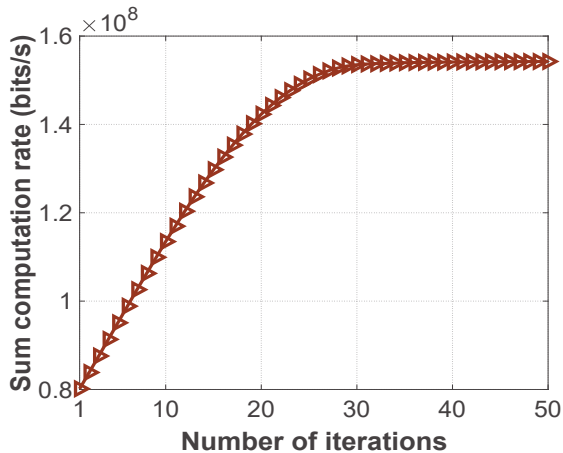
Fig. 5: An example of the convergence behavior of the resource allocation algorithm for the partial offloading mode in a multiuser UAV-aided wireless powered MEC system.
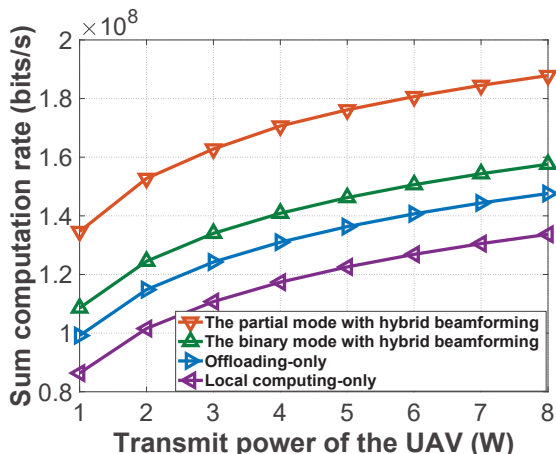

(a)

(b)

Fig. 7: The performance of two proposed resource allocation algorithms: (a) The sum computation rate versus the transmit power of the UAV under the partial offloading mode; (b) The sum computation rate versus the transmit power of the UAV under the binary offloading mode.

Fig. 6: The sum computation rate of all IoT devices versus the transmit power of the UAV under different resource allocation schemes.

our proposed scheme is 8 dB more than the gain of sidelobes.

Next, we investigate the convergence behavior of the resource allocation algorithm for solving problem (P4). We set $P_0 = 1$ and $K = 4$. The convergence behavior of the proposed algorithm is characterized by illustrating how the sum computation rate behaves with iteration times. As seen in Fig. 5, since the proposed resource allocation algorithm for the partial offloading mode involves a joint WPT time allocation and computation resource scheduling procedure, the sum computation rate converges to a fixed value after around 28 iterations.

We then show the sum computation rate of the two resource allocation algorithms under partial offloading pattern and binary offloading pattern, and compare them to the "offloading-only" scheme and the "local computing-only" scheme. The number of IoT devices is fixed to $K = 4$, while the transmit power of the UAV varies from 1 W to 8 W. As shown in Fig. 6, the resource allocation algorithm under the partial offloading pattern achieves a high sum computation rate compared to the binary offloading mode. This is because all the IoT
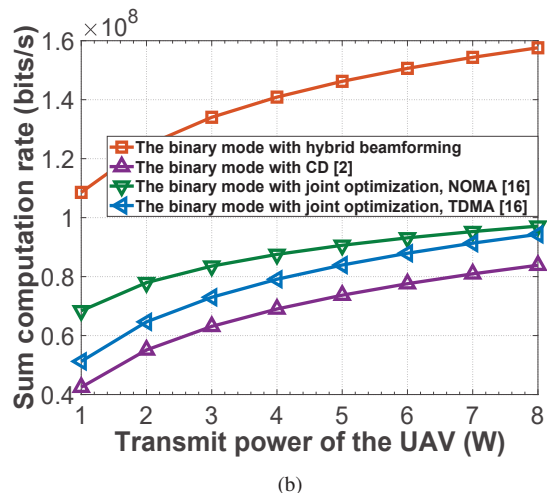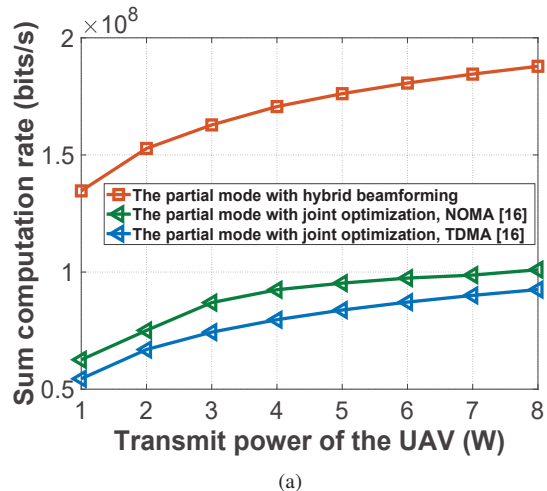
devices can flexibly choose the computing mode depending on their channel conditions in the partial offloading pattern, whilst the computation task is implemented either locally at the IoT devices or at the UAV in the binary offloading mode. Moreover, the "offloading-only" scheme can achieve higher performance compared with the "local computing-only" scheme when the transmit power becomes large.

In the next simulation, we investigate the sum computation rate for both partial and binary offloading patterns with different transmit powers. To show the computation performance, we compare with the "CD" algorithm in [2] and the "joint optimization" algorithm in [16]. We assume that there are $K = 4$ IoT devices and $P_0 = 1$. From Fig. 7, it can be seen that the sum computation rates achieved by our two proposed resource allocation algorithms outperform both the "CD" algorithm and the "joint optimization" algorithm. This is due to the fact that both the "CD" algorithm and the "joint optimization" algorithm only use a single antenna for WPT. In particular, our proposed resource allocation algorithms enable the UAV-mounted antenna array to form multiple beams to
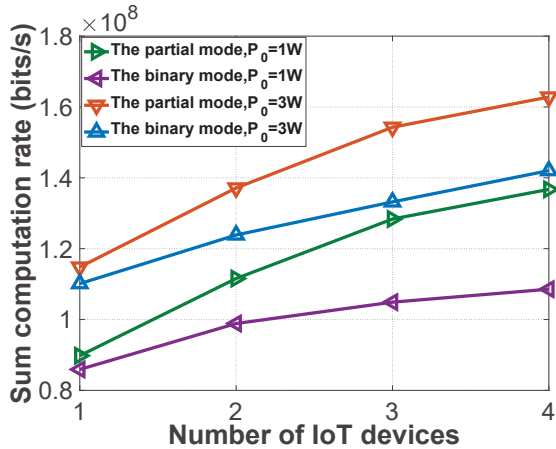
Fig. 8: The sum computation rate of all IoT devices versus the number of IoT devices under different resource allocation schemes.

Fig. 9: The sum computation rate of all IoT devices versus the minimum altitude of the UAV under different resource allocation schemes.

charge IoT devices which can compensate for the high propagation loss, which thereby improves the sum computation rate. Moreover, our proposed algorithms employ NOMA which enables multiple IoT devices to transmit their tasks to the UAV simultaneously, and thus improve the performance in terms of the sum computation rate.

We then study the sum computation rate of the two proposed resource allocation algorithms under different number of IoT devices. In Fig. 8, the sum computation rate achieved by the two resource allocation algorithms are monotonically non-decreasing with the number of IoT devices. Particularly, the sum computation rate increases with a small quantity of IoT devices, i.e., $K < 3$, and then saturates when $K \geq 3$. This is because the interference is also increasing with the growing number of IoT devices, and the sum computation rate is still limited in this case.

Finally, we investigate the sum computation rate versus the minimum altitude of the UAV for the two resource allocation algorithms. As shown in Fig. 9, both resource allocation algorithms achieve good performance with a lower minimum altitude, i.e., $h_{min} \leq 10$, but achieve poor performance when $h_{min} > 10$. This is due to the fact that increasing the minimum altitude of the UAV will degrade the channel quality of IoT devices, and thus restrict the improvement of the sum computation rate.

VII. CONCLUSION

This paper exploited hybrid beamforming and NOMA for enhancing the computation performance of UAV-aided wireless-powered MEC networks. By considering both partial and binary offloading patterns, we maximized the sum computation rate at all the IoT devices by jointly optimizing the UAV's 3D position, hybrid beamforming design and computation resource allocation. To tackle these problems, we first presented a SUCM-based placement optimization algorithm to derive the closed-form solution of the 3D placement of the UAV. Subsequently, a learning-based two-stage hybrid beamforming algorithm was proposed for beamforming design. Furthermore, two resource allocation algorithms for
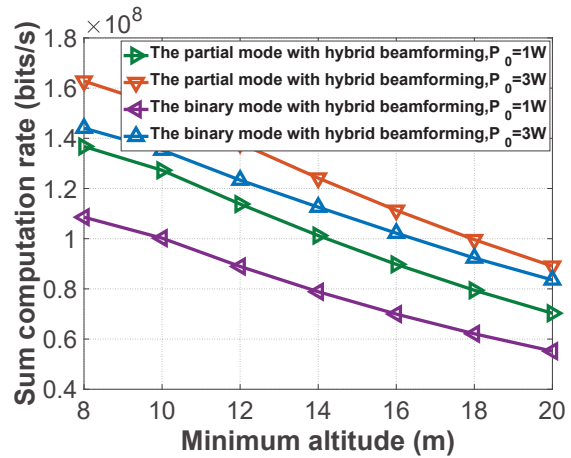
two computing modes were then presented to maximize the sum computation rate. Numerical results demonstrated that the sum computation rate of all the IoT devices can be significantly enhanced by the designed resource allocation algorithms compared to the benchmark schemes.

APPENDIX A
PROOF OF PROPOSITION 2

By adding a set of non-negative dual variables, λ_k, $k = 1, \cdots, K$, associated with the energy harvesting constraints for the IoT devices in problem (P4.2), the Lagrangian function of problem (P4.2) can be expressed as

$$
\begin{aligned}
& L(\lambda_k, f_k, P_k) \\
& = \sum_{k=1}^{K} \frac{f_k t_k}{C_k T} + B(1-a) \log_2 \left(\frac{\sum_{i=1}^{K} P_i g_i + N_0}{N_0} \right) \\
& + \sum_{k=1}^{K} \lambda_k \left[aT\xi_0 P_0 |\mathbf{h}_k^H \mathbf{F} \mathbf{w}_k|^2 - \tau_k f_k^3 t_k - P_k(1-a)T \right]
\end{aligned}
\tag{39}
$$

Then, the derivatives of $L(\lambda_k, f_k, P_k)$ with respect to f_k and P_k are given by

$$
\frac{\partial L(\lambda_k, f_k, P_k)}{\partial f_k} = \frac{t_k}{C_k T} - 3\lambda_k \tau_k f_k^2 t_k,
\tag{40}
$$

$$
\frac{\partial L(\lambda_k, f_k, P_k)}{\partial P_k} = \frac{B(1-a)g_k}{\left(\sum_{m=k}^{K} P_m g_m + N_0\right) \ln 2} - (1-a)T.
\tag{41}
$$

By applying the Karush-Kuhn-Tucher (KKT) conditions [33], we can obtain the optimal solutions of problem (P4.2)

$$
f_k^* = \sqrt{\frac{1}{3\lambda_k \tau_k C_k T}},
\tag{42}
$$

$$
\sum_{m=k}^{K} P_m^* g_m = \left[\frac{B g_k}{\lambda_k T \ln 2} - N_0 \right]^{+}.
\tag{43}
$$

Therefore, this completes the proof of Proposition 2.

APPENDIX B
PROOF OF PROPOSITION 3

Since the local computation rate of IoT devices $r_{L,k}^{bin}$ is increasing with respect to t_k and f_k, the maximum $r_{L,k}^{bin}$ can be obtained from (47a) with $t_k^* = T$. This implies that the devices compute during the whole period T. Substituting $t_k^* = T$ into (47b) and applying $0 \leq f_k \leq f_{max}$ yields the following optimal CPU frequency as $f_k^* = \min\left(\left(\frac{a\xi_0 P_0 |\mathbf{h}_k^H \mathbf{F} \mathbf{w}_k|^2}{\tau_k} \right)^{\frac{1}{3}}, f_{max} \right)$. By combining this result with (12), we finally obtain $f_k^* = \left(\frac{a\xi_0 P_0 |\mathbf{h}_k^H \mathbf{F} \mathbf{w}_k|^2}{\tau_k} \right)^{\frac{1}{3}}$. Therefore, this completes the proof of Proposition 3.

REFERENCES

[1] Z. Liang, Y. Liu, T. Lok, and K. Huang, "Multiuser computation offloading and downloading for edge computing with virtualization," *IEEE Trans. Wireless Commun.*, vol. 18, no. 9, pp. 4298–4311, Sep. 2019.

[2] S. Bi and Y. J. Zhang, "Computation rate maximization for wireless powered mobile-edge computing with binary computation offloading," *IEEE Trans. Wireless Commun.*, vol. 17, no. 6, pp. 4177–4190, Jun. 2018.

[3] M. Liu and Y. Liu, "Price-based distributed offloading for mobile-edge computing with computation capacity constraints," *IEEE Wireless Commun. Lett.*, vol. 7, no. 3, pp. 420–423, Jun. 2018.

[4] W. Feng, J. Tang, Y. Yu, J. Song, N. Zhao, G. Chen, K.-K. Wong, and J. Chambers, "UAV-enabled SWIPT in IoT networks for emergency communications," *IEEE Wireless Commun.*, to be published, DOI: 10.1109/MWC.001.1900656.

[5] Z. Ding, X. Lei, G.K. Karagiannidis, R. Schober, J. Yuan, and V.K. Bhargava, "A survey on non-orthogonal multiple access for 5G networks: Research challenges and future trends," *IEEE J. Sel. Areas Commun.*, vol. 35, no. 10, pp. 2181–2195, Oct. 2017.

[6] F. Wang, J. Xu, and Z. Ding, "Multi-antenna NOMA for computation offloading in multiuser mobile edge computing systems," *IEEE Trans. Commun.*, vol. 67, no. 3, pp. 2450–2463, Mar. 2019.

[7] Z. Yang, C. Pan, J. Hou, and M. Shikh-Bahaei, "Efficient resource allocation for mobile-edge computing networks with NOMA: Completion time and energy minimization," *IEEE Trans. Commun.*, vol. 67, no. 11, pp. 7771–7784, Nov. 2019.

[8] Y. Ye, L. Shi, H. Sun, R. Q. Hu, and G. Lu, "System-centric computation energy efficiency for distributed NOMA-based MEC networks," *IEEE Trans. Veh. Technol.*, vol. 69, no. 8, pp. 8938–8948, Aug. 2020.

[9] W. Feng, N. Zhao, S. Ao, J. Tang, X. Zhang, Y. Fu, D.K.C. So, and K.-K. Wong, "Joint 3D trajectory design and time allocation for UAV-enabled wireless power transfer networks," *IEEE Trans. Veh. Technol.*, to be published, DOI: 10.1109/TVT.2020.2972133.

[10] T. Zhang, Y. Xu, J. Loo, D. Yang, and L. Xiao, "Joint computation and communication design for UAV-assisted mobile edge computing in IoT," *IEEE Trans. Ind. Informat.*, vol. 16, no. 8, pp. 5505–5516, Aug. 2020.

[11] Q. Hu, Y. Cai, G. Yu, Z. Qin, M. Zhao, and G. Y. Li, "Joint offloading and trajectory design for UAV-enabled mobile edge computing systems," *IEEE Internet Things J.*, vol. 6, no. 2, pp. 1879–1892, Apr. 2019.

[12] J. Hu, M. Jiang, Q. Zhang, Q. Li, and J. Qin, "Joint optimization of uav position, time slot allocation, and computation task partition in multiuser aerial mobile-edge computing systems," *IEEE Trans. Veh. Technol.*, vol. 68, no. 7, pp. 7231–7235, Jul. 2019.

[13] Y. Wang, Z. Ru, K. Wang, and P. Huang, "Joint deployment and task scheduling optimization for large-scale mobile users in multi-UAV-enabled mobile edge computing," *IEEE Trans. Cybern.*, vol. 50, no. 9, pp. 3984–3997, Sep. 2020.

[14] J. Tang, A. Shojaeifard, D. K. C. So, K. Wong, and N. Zhao, "Energy efficiency optimization for CoMP-SWIPT heterogeneous networks," *IEEE Trans. Commun.*, vol. 66, no. 12, pp. 6368–6383, Dec. 2018.

[15] J. Tang, D. K. C. So, N. Zhao, A. Shojaeifard, and K. Wong, "Energy efficiency optimization with SWIPT in MIMO broadcast channels for Internet of Things," *IEEE Internet Things J.*, vol. 5, no. 4, pp. 2605–2619, Aug. 2018.

[16] F. Zhou, Y. Wu, R. Q. Hu, and Y. Qian, "Computation rate maximization in UAV-enabled wireless-powered mobile-edge computing systems," *IEEE J. Sel. Areas Commun.*, vol. 36, no. 9, pp. 1927–1941, Sep. 2018.

[17] F. Zhou and R. Q. Hu, "Computation efficiency maximization in wireless-powered mobile edge computing networks," *IEEE Trans. Wireless Commun.*, vol. 19, no. 5, pp. 3170–3184, May 2020.

[18] Y. Liu, K. Xiong, Q. Ni, P. Fan, and K. B. Letaief, "UAV-assisted wireless powered cooperative mobile edge computing: Joint offloading, CPU control, and trajectory optimization," *IEEE Internet Things J.*, vol. 7, no. 4, pp. 2777–2790, Apr. 2020.

[19] F. Wang, J. Xu, and S. Cui, "Optimal energy allocation and task offloading policy for wireless powered mobile edge computing systems," *IEEE Trans. Wireless Commun.*, vol. 19, no. 4, pp. 2443–2459, Apr. 2020.

[20] J. Du, W. Xu, Y. Deng, A. Nallanathan, and L. Vandendorpe, "Energy-saving UAV-assisted multiuser communications with massive MIMO hybrid beamforming," *IEEE Commun. Lett.*, vol. 24, no. 5, pp. 1100–1104, May 2020.

[21] I. Ahmed, H. Khammari, A. Shahid, A. Musa, K. S. Kim, E. De Poorter, and I. Moerman, "A survey on hybrid beamforming techniques in 5G: Architecture and system model perspectives," *IEEE Commun. Surveys Tuts.*, vol. 20, no. 4, pp. 3060–3097, 4th Quart., 2018.

[22] Y. Sun, D. W. K. Ng, Z. Ding, and R. Schober, "Optimal joint power and subcarrier allocation for full-duplex multicarrier non-orthogonal multiple access systems," *IEEE Trans. Commun.*, vol. 65, no. 3, pp. 1077–1091, Mar. 2017.

[23] Z. Wei, L. Yang, D. W. K. Ng, J. Yuan, and L. Hanzo, "On the performance gain of NOMA over OMA in uplink communication systems," *IEEE Trans. Commun.*, vol. 68, no. 1, pp. 536–568, Jan. 2020.

[24] Y. Pochet and L. A. Wolsey, *Production planning by mixed integer programming*, Berlin, Germany: Springer, 2006.

[25] S. Boyd and L. Vandenberghe, *Convex Optimization*. Cambridge, U.K.: Cambridge Univ. Press, 2004.

[26] H. Tuy and F. A. Al-Khayyal, "Global optimization of a nonconvex single facility location problem by sequential unconstrained convex minimization," *J. Global Optim.*, vol. 2, no. 1, pp. 61–71, Mar. 1992.

[27] I. Tsevendorj, "Piecewise-convex maximization problems," *J. Global Optim.*, vol. 21, no. 1, pp. 1–14, Sep. 2001.

[28] J. Borwein and A. S. Lewis, *Convex Analysis and Nonlinear Optimization: Theory and Examples*. New York, NY, USA: Springer-Verlag, 2006.

[29] J. Xu and R. Zhang, "A general design framework for MIMO wireless energy transfer with limited feedback," *IEEE Trans. Signal Process.*, vol. 64, no. 10, pp. 2475–2488, May 2016.

[30] C. A. Balanis, *Antenna Theory: Analysis and Design*. New York, NY, USA: Wiley, 2016.

[31] Q. Zhang and H. Li, "MOEA/D: A multi-objective evolutionary algorithm based on decomposition," *IEEE Trans. Evol. Comput.*, vol. 11, no. 6, pp. 712–731, Dec. 2007.

[32] R. Storn and K. Price, "Differential evolution: A simple and efficient heuristic for global optimization over continuous spaces," *J. Global Optimization*, vol. 11, no. 4, pp. 341–359, Dec. 1997.

[33] S. Boyd and L. Vandenberghe, *Convex Optimization*. Cambridge, U.K.: Cambridge Univ. Press, 2004.

[34] D. P. Palomar and M. Chiang, "A tutorial on decomposition methods for network utility maximization," *IEEE J. Sel. Areas Commun.*, vol. 24, no. 8, pp. 1439–1451, Aug. 2006.

[35] M. Grant and S. Boyd, "CVX: Matlab software for disciplined convex programming, version 2.2," Jan. 2020 [Online]. Available: http://cvxr.com/cvx.

[36] P. D. Diamantoulakis, K. N. Pappi, Z. Ding, and G. K. Karagiannidis, "Wireless-powered communications with non-orthogonal multiple access," *IEEE Trans. Wireless Commun.*, vol. 15, no. 12, pp. 8422–8436, Dec. 2016.